Energy & Buildings 274 (2022) 112422

Contents lists available at ScienceDirect

Energy & Buildings

journal homepage: www.elsevier.com/locate/enb

A novel algorithm for optimal equipment scheduling and dispatch of chilled water systems with ice thermal storage

I. Al-Aali *, A. Narayanaswamy, V. Modi

Mechanical Engineering Department, Columbia University, New York City 10027, United States

ARTICLE INFO

Article history:
Received 2 June 2022
Revised 17 August 2022
Accepted 21 August 2022
Available online 27 August 2022

Keywords:
Ice storage
Thermal storage
Chilled water system
Optimal control
Chiller Sequencing
Meta-heuristic optimization
Load shifting
Peak shaving

ABSTRACT

Using thermal energy storage in chilled water systems can reduce electricity bill charges and required chiller cooling capacity through load shifting and peak demand shavings. As opposed to simple heuristic strategies, optimal storage dispatch maximizes savings by considering the time of use tariffs and system efficiency. In this paper, we propose a solution to the optimal equipment scheduling and storage dispatch problem of multi-chiller chilled water systems with ice thermal storage. We model the system in a bi-level optimization formulation that is solved using the genetic algorithm. The upper level minimizes daily operation costs and decides the storage dispatch amount over the next 24 h. The decided upon dispatch amount is fed to the lower-level optimizer to solve the equipment scheduling problem sequentially and return the corresponding system power consumption over the next 24 h. Flowrate and energy balancing constraints are handled using the penalty function method. Tuning of the penalty factors and genetic algorithm parameters significantly diminished and eliminated the problem of premature convergence. While the genetic algorithm is computationally taxing, we reduced the run time to 1–2 min by pre-solving the lower-level problem under various input conditions and tri-linearly interpolating between them. We compared the developed optimal control strategy to two commonly used heuristic storage dispatch strategies: chiller priority control and storage priority control in three scenarios of cooling demand under a time of use electricity pricing. Our model suggests optimal control reduces cost and energy by 11–14% and 10–12%, respectively, relative to storage priority control, and 16–33% and 1–9%, respectively, relative to chiller priority control. In a scenario with a demand charge, optimized control reduces demand charges by 17% relative to storage priority and 26% relative to chiller priority control. The gains from the proposed approach are augmented when a more sophisticated tariff structure is present.

© 2022 Elsevier B.V. All rights reserved.

1. Introduction

The development of air conditioning allowed for maintaining indoor comfort irrespective of outdoor ambient conditions. It is primarily accomplished using energy-intensive technologies powered by electrical grids dominated by carbon-based energy sources. The soaring demand for air conditioning necessitates a more sustainable approach to cooling to mitigate further warming of the earth's atmosphere due to increased emissions of greenhouse gases. This includes using renewable energy sources with energy storage combined with passive cooling design, energy efficiency, and optimal resource management. In regions with a time of use (TOU) electricity pricing or demand charges, thermal energy storage can be used to reduce building peak electricity demand and the required chiller cooling capacity and in load shifting. In that mode of operation, the thermal storage is charged during the off-peak period, typically at night, and discharged during the on-peak period, typically in the afternoon, making it suitable for use in schools, offices, and other buildings with dominant daytime cooling needs. In this paper, we propose a solution to the optimal scheduling and dispatch problem of multi-chiller chilled water systems with ice thermal storage under TOU rates.

The literature is rich with attempts to solve the chilled water system's scheduling problems [1–10]. The bulk of literature neglects the roles of auxiliary components and only considers the problem of sequencing of chillers. For these problems, they tend to assume a fixed water supply and condenser temperatures. This simplifies the chiller model to a cubic or often a quadratic function of their loading. Various optimization strategies are used to solve these problems, ranging from simple linear to quadratic programming and *meta*-heuristic optimization strategies like genetic algorithm and particle swarm optimization. The most detailed model

* Corresponding author.
E-mail addresses: iaa2111@columbia.edu (I. Al-Aali), arvind.narayanaswamy@columbia.edu (A. Narayanaswamy), modi@columbia.edu (V. Modi).

https://doi.org/10.1016/j.enbuild.2022.112422
0378-7788/© 2022 Elsevier B.V. All rights reserved.

Nomenclature

Parameters

Symbol	Meaning
$\dot{m}$	Flowrate, kg/s
T	Temperature, °C
COP	Coefficient of Performance, dimensionless
$\dot{Q}$	Heat transfer rate, kW
R	Chillers heat exchanger effective thermal resistance, K/kW
ΔS	Entropy generation rate, kW/K
$\dot{H}$	Rate of change of enthalpy, kW
P	Power, kW
k	Pumps/fans constant, kW
c^e	Time of use electricity rates, $/kWh
c^p	Specific heat, kJ/kg.°C
C^{is}	Ice storage thermal capacity, kJ
ρ	Density, kg/m3
h	Specific enthalpy, kJ/kg
η	Efficiency, dimensionless
x	Evaporator refrigerant quality, dimensionless
PLR	Part-load ratio, dimensionless
SoC	State of charge, dimensionless
VSD	Angular speed, % of maximum speed
A	Area, m^2
N^{row}	Number of coils rows
V	Fluid face velocity, m/s

Superscripts

max	Maximum
refg	Refrigerant
des	Design conditions
chl	Chiller
pp	Primary pump
cp	Condenser pump
sp	Secondary pump
cf	Coil fan
twr	Cooling Tower
cc	Cooling coils
Sys	System
sw	Chiller evaporator leaving water
bsw	Blended chillers evaporator leaving water
brw	Blended chillers evaporator returning water
cw	Chiller condenser water
bcw	Blended chillers condenser water
bcsw	Blended chillers condenser entering water
bcrw	Blended chillers condenser leaving water
ccsw	Cooling coil supply water
ccrw	Cooling coil return water
isw	Ice storage supply water
cca	Cooling coil air
twra	Cooling tower air
VSD	Variable speed drive
m	Motor
a	Air
w	Water
ice	Ice
is	Ice storage
ai	Coil inlet air
ae	Coil exit air
s	Sensible
l	Latent
$\mathscr{D}$	Demand
dp	Coil air dew-point
dry	Dry section of the coil
wet	Wet section of the coil
int	Internal
ext	External
sat	Saturated with water
wb	Ambient air wet-bulb
is	Ice storage
fg	Latent heat of evaporation
sf	Latent heat of fusion

Index Sets

t	Time step index set denoted by $\mathscr{T}$
i	Chiller index set denoted by $\mathscr{I}$
n	Cooling tower index set denoted by $\mathscr{N}$
s	Secondary pump index set denoted by $\mathscr{S}$
z	Training data index set denoted by $\mathscr{Z}$

Decision Variables

$T^{sw}_{t,i}$	Leaving chilled water temperature for chiller i at time step t, °C
T^{bcsw}_{t}	Entering condenser water temperature for chillers at time step t, °C
$\dot{m}^{isw}_{t}$	Storage water flowrate at time step t, kg/s
VSD^{cf}_{t}	Cooling coil fan motor speed at time step t, % of maximum speed
VSD^{sp}_{t}	Secondary pump motor speed at time step t, % of maximum speed
VSD^{twr}_{t}	Cooling tower fan motor speed at time step t, % of maximum speed
$ON^{chl}_{t,i}$	Chiller power switch for chiller i at time step t, binary
$ON^{twr}_{t,n}$	Fan power switch for cooling tower n at time step t, binary

found in the literature was developed by Zhang et al. [11]. The formulation captures the complex behavior of chillers and cooling towers using regression-based models and takes supply and condenser water temperatures as decision variables. The considered solution approach is near-optimal using sequential quadratic programming. In another work, Zhang et al. [12] consider the effect of minimum up/down time constraints on the optimization. Their work suggests that minimum up/down time significantly increases the complexity of the problem with little return in cost minimization, and it is best handled heuristically post-computation. Trautman et al. [13] formulated a detailed chilled water system model optimizing the condenser water pump and tower fan speed. Their model results suggest optimal tower fan speed can achieve 12–15 % energy savings, while condenser pump control had negligible energy savings.

Much attention has also been given to the scheduling problem with thermal energy storage [14–23]. A more sophisticated model and optimization strategy are often used in these problems. Lee et al. [15] used *meta*-heuristic particle swarm optimization to minimize ice storage life cycle cost for a single water-cooled chiller system. Chen et al. [17] utilized the dynamic programming method to optimize a chilled water system with ice storage. Zhu et al. [20] proposed a bi-level optimization strategy to optimize the capacity and operation of a multi-chiller chilled water system with electric and thermal energy storage. The optimization strategy employs a *meta*-heuristic genetic algorithm for the upper level and mixed-

integer linear programming for the lower level with piece-wise linearization. The study suggests that energy storage can significantly reduce cost and increase renewable penetration in the grid because of load shifting. Kamal et al. [23] used an evolutionary algorithm to optimize a multi-chiller chilled water system with ice and chilled water storage for load shifting and cost reduction. Storage was found to reduce cost and equipment size.

A prevalent solution strategy in the literature is the genetic algorithm, which is a type of *meta*-heuristic evolutionary optimization strategy inspired by the theory of evolution. The algorithm can work with non-convex and non-continuous problems [24–26], typically confronted with equipment scheduling problems. They explore the solution space by using a population of potential solutions. The algorithm selects the fittest individuals to produce the next generation of solutions. Over multiple iterations, the algorithm evolves toward a globally optimal solution.

In this paper, we consider physics-based steady-state models for the ice thermal storage and each of the key power-consuming components, including the chillers, cooling towers, water pumps, and cooling coil fans. We formulate the modeled system into a bi-level optimization problem solved using genetic algorithm at both levels. The upper level minimizes daily operation costs and decides the storage dispatch amount over the next 24 h. The decided upon dispatch amount is fed to the lower-level optimizer to solve the equipment scheduling problem sequentially and return the corresponding system power consumption at each hour. Balancing constraints derived from the conservation of mass and energy in the lower-level problem are handled using the penalty function method. Tuning of the penalty factors and genetic algorithm parameters significantly diminished and eliminated the problem of premature convergence. While computationally taxing, the run time for the proposed approach can be reduced to 1–2 min by pre-solving the lower-level problem under a range of input conditions and tri-linearly interpolating between them. The lower-level scheduling problem is influenced by the cooling demand, the ambient condition, and storage use. The proposed decomposition and tuning solution strategy provides a reasonably scalable and robust approach that can be used on highly non-linear space cooling and heating problems, thereby negating the need for simplistic models.

In this study, we consider the scheduling problem of a chilled water system with multi-chillers and ice thermal storage in a primary-secondary configuration shown in Fig. 1. Primary-secondary flow configuration is a standard chilled water system configuration used on small to large buildings [27–29]. In this configuration, the secondary (distribution) loop is decoupled from the primary (production) loop. The chillers operate with their respective fixed-speed pumps to maintain design flow. Variable speed pumps modulate the water supply to the coil to meet the building cooling load. Surplus water flows back to the chillers through the bypass and blends with the coil's return water. The considered system is comprised of 3 chillers, two 212-tons Carrier 19XR chillers with VSD, and one 153-tons Trane RTHB chiller, with a cumulative chiller cooling capacity of 570 tons, two 360 tons cooling towers, 1600 ton-hr internal melt ice storage for a design building cooling demand of 730 tons.

In section 2, we present the methodology. First, we outline the employed model for each key component and then lay out the overall problem formulation and the developed optimization strategy. In section 3, we solve the problem for three scenarios of cooling demand under TOU electricity pricing. The proposed approach is compared to two commonly used heuristic strategies for storage use: chiller priority control and storage priority control. Lastly, the study is summarized in section 4.

2. Methodology

2.1. Components modeling

2.1.1. Chillers

Chillers are the dominant power-consuming component in chilled water systems. The performance of chillers is a function of their loading and supply and condenser temperatures. We consider a widely used simple model first developed by Gordon-Ng [31] to predict electric chillers' coefficient of performance (COP) using the first and second laws of thermodynamics. A modification to the model was proposed by Jian and Reddy [32] to include a term representing entropy generation rate due to irreversibility that is dependent on loading ($\Delta S_i^{intQ}\dot{Q}_{t,i}^{chl}/\dot{Q}_i^{des}$) in addition to a constant entropy generation rate term (ΔS_i^{int}) which slightly improves its prediction capabilities. The modified Gordon-Ng model is as follows:

$$\frac{T_{t,i}^{sw}}{T_t^{bcsw}}\left[1+\frac{1}{COP_{t,i}}\right]=1+\frac{T_{t,i}^{sw}\left(\Delta S_i^{int}+\Delta S_i^{intQ}\frac{\dot{Q}_{t,i}^{chl}}{\dot{Q}_i^{des}}\right)}{\dot{Q}_{t,i}^{chl}}+\frac{\dot{Q}_i^{leak,eqv}\left(T_t^{bcsw}-T_{t,i}^{sw}\right)}{T_t^{bcsw}\dot{Q}_{t,i}^{chl}}+\frac{R_i\dot{Q}_{t,i}^{chl}}{T_t^{bcsw}}\left[1+\frac{1}{COP_{t,i}}\right] \quad (1)$$

and the chiller loading is given by:

$$\dot{Q}_{t,i}^{chl}=\dot{m}_i^{sw}c^{p,sw}\left(T_t^{brw}-T_{t,i}^{sw}\right) \quad (2)$$

i is the chiller index set $\{1, 2, 3\}$ denoted by $\mathscr{I}$, and t is the time-step index set $\{1, 2, 3, \cdots, 24\}$ denoted by $\mathscr{T}$. $T_{t,i}^{sw}$ and T_t^{brw} are the chiller evaporator leaving and returning water-glycol mixture temperatures, respectively, T_t^{bcsw} is the condenser entering temperature, $\dot{m}_i^{sw}$ is the chiller evaporator water flowrate, $c^{p,sw}$ is the water-glycol mixture specific heat, and $\dot{Q}_i^{des}$ is the chiller cooling capacity at design conditions. The parameters in Gordon's model: $\dot{Q}_i^{leak,eqv}$ is the heat leak into the evaporator from the ambient and out of the condenser into the ambient, the latter being less significant; R_i is the equivalent thermal resistance for the evaporator and condenser heat exchangers and dominates the chiller performance at high chiller loading; ΔS_i^{int} is internal entropy generation rate and dominates performance at low loading conditions. ΔS_i^{int}, ΔS_i^{intQ}, R_i and $\dot{Q}_i^{leak,eqv}$ are obtained using least square linear regression from known chiller performance data. Chiller power consumption can then be calculated from the predicted COP:

$$P_{t,i}^{chl}=\frac{\dot{Q}_{t,i}^{chl}}{COP_{t,i}}ON_{t,i}^{chl} \quad (3)$$

$ON_{t,i}^{chl}$ are binary decision variables for the chillers power switch. We use the public library of chiller data in EnergyPlus given in a regression-based model with three polynomial curves using the DOE-2 model [33,34]. The first curve (called *CAPFT* in EnergyPlus) describes the influence of entering evaporator and condenser temperatures on the cooling capacity. The second curve (called *EIRFT* in EnergyPlus) describes the influence of entering evaporator and condenser temperatures on electric power consumption. The third curve (called *EIRFPLR* in EnergyPlus) describes the influence of the

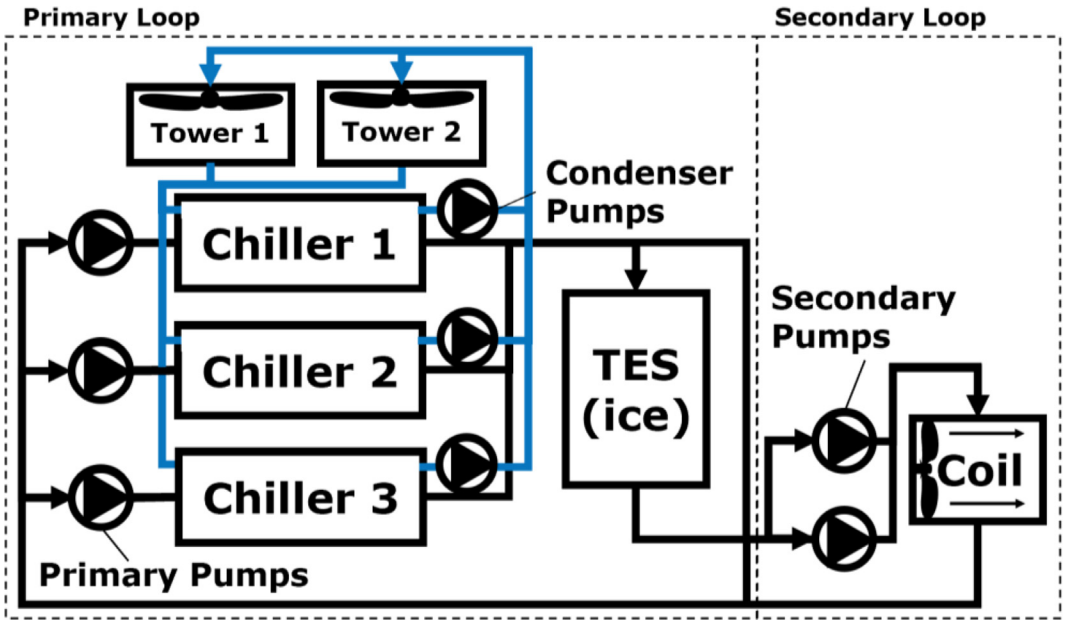

Fig. 1. Considered chilled water system in a primary-secondary configuration with three water-cooled chillers (two 212-tons Carrier 19XR chillers with VSD and one 153-tons Trane RTHB chiller), two shared cooling towers (360 tons each), and ice thermal storage (1600 ton-hr). The building is represented in a single coil with the respective aggregate cooling load.

chiller loading on electric power consumption. However, the given three polynomial curves are only valid within narrow ranges of temperatures. They cannot predict chiller performance at low evaporator temperatures associated with ice storage charging or high condenser temperatures associated with hot and humid climates. We uniformly sample the COP described by the three polynomial curves within the given range of condenser and supply temperatures and loading conditions. Least-square linear regression is applied between the model's predicted COP and sampled COP from EnergyPlus to determine ΔS^{int}, ΔS^{intQ}, R and $Q^{leak,eqv}$. The considered system is comprised of three low-flow chillers with a design ΔT of 10 °C in the evaporator and condenser; two 212-tons centrifugal chillers with VSD (Carrier 19XR), and one 153-tons screw chiller (Trane RTHB). The characteristics of the selected chillers can be found in Tables 2 and 3 in the Appendix. The COP predicted by the modified Gordon-Ng model compared to the sampled COP from EnergyPlus is shown in Fig. 2 (A) for Trane RTHB chiller. The modified Gordon-Ng model often underpredicts the COP by no more than 10 %.

Not only the performance of a chiller varies with operating conditions but too its available cooling capacity. A reduction in supply temperature or an increase in condenser temperature depresses the cooling capacity. On the contrary, re-setting the supply temperature or reducing the condensing temperature enhances the evaporator capacity. However, the utility from the increase in evaporator heat transfer capacity is ultimately constrained by the compressor's ability to support the required flow and pressure head. Centrifugal compressors are constant pressure variable flow machines and do not experience significant gain or loss in capacity when the pressure differential is varied. On the other hand, positive displacement compressors are constant flow variable pressure machines and experience dramatic gain or loss in capacity when the pressure differential is varied [35,36]. The refrigerant saturation density, which affects the mass flowrate, becomes the dominant factor in depressing the chiller cooling capacity in ice-making mode. Chillers can experience as much as 30–40 % loss in capacity when operating in ice-making mode. A simple yet powerful approach is to predict the chiller cooling capacity from the

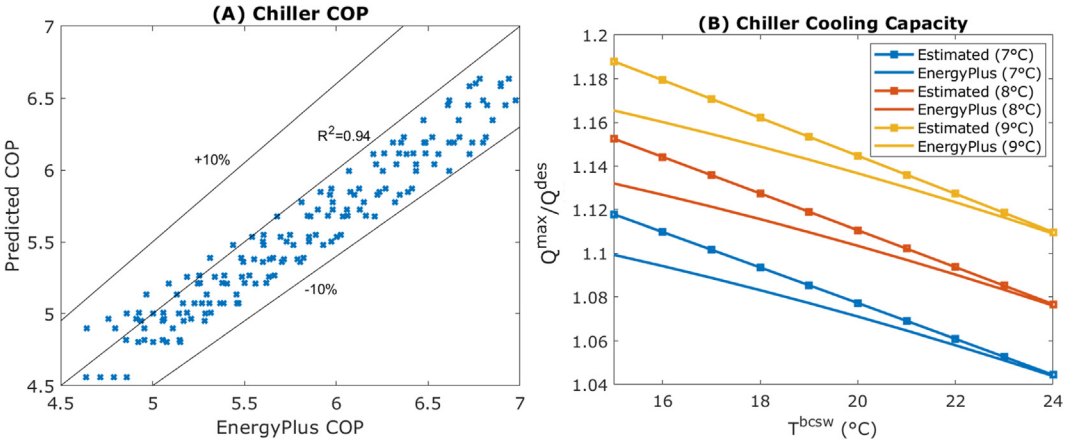

Fig. 2. Trane RTHB screw chiller: (A) Predicted COP using the modified Gordon-Ng model versus COP from EnergyPlus uniformly sampled over the entire given range of supply and condenser temperatures and chiller loading, and (B) Estimated cooling capacity ratio from refrigerant thermal capacity versus from EnergyPlus.

refrigerant thermal capacity under the specified conditions. The cooling capacity ratio is defined as the ratio of available to design cooling capacity:

$$\frac{\dot{Q}_{t,i}^{max}}{\dot{Q}_{i}^{des}} = \frac{h_{t,i}^{refg,fg}}{h_{i}^{refg,fg,des}} \frac{1 - x_{t,i}^{refg}}{1 - x_{i}^{refg,des}} \frac{\rho_{t,i}^{refg}}{\rho_{i}^{refg,des}} \tag{4}$$

$h_{t,i}^{refg,fg}$ is the refrigerant enthalpy of vaporization, $\rho_{t,i}^{refg}$ is saturated vapor density, and $x_{t,i}^{refg}$ is the quality of the refrigerant vapor mixture in the evaporator. Parameters in the denominator of Equation (4) are evaluated at reference or design refrigerant temperatures. The refrigerant and water temperatures are related by the approach temperature, which is the difference between leaving water and refrigerant temperatures in the evaporator and condenser. It is on the order of 0.5–2 °C for modern chillers [37,38]. While the approach temperatures depend on the load, the variations are too small to impact the chiller cooling capacity. The estimated cooling capacity ratio must not exceed the chiller's compressor capacity ratio, which yields the following expression for the cooling capacity ratio:

$$\frac{\dot{Q}_{t,i}^{max}}{\dot{Q}_{i}^{des}} = min\left[\frac{\dot{Q}_{i}^{chl,max}}{\dot{Q}_{i}^{des}}, \frac{h_{t,i}^{refg,fg}}{h_{i}^{refg,fg,des}} \frac{1 - x_{t,i}^{refg}}{1 - x_{i}^{refg,des}} \frac{\rho_{t,i}^{refg}}{\rho_{i}^{refg,des}}\right] \tag{5}$$

$\dot{Q}_{i}^{chl,max}$ is the maximum chiller cooling rate the compressor allows at a given supply and condenser water temperatures obtained from *CAPFT* from EnergyPlus. A comparison of predicted cooling capacity ratios and capacity ratios from EnergyPlus is in Fig. 2 for Trane RTHB screw chiller (B). A slight difference of no more than 3 % is observed between the estimated and known cooling capacity ratios.

2.1.2. Pumps and fans

Chiller pumps (primary and condenser) are fixed-speed pumps controlled to maintain the design evaporator and condenser water flowrates and only operate with their associated chiller. Secondary pumps are speed controlled to deliver the required flowrate to satisfy the building cooling load. Excess water returns to the chiller flow through the decoupler. The power required by fixed-speed pumps is constant.

$$P_{t,i}^{pp} = k_{i}^{pp} ON_{t,i}^{chl} \tag{6}$$

$$P_{t,i}^{cp} = k_{i}^{cp} ON_{t,i}^{chl} \tag{7}$$

Superscript *pp* and *cp* refer to primary and condenser pumps, respectively, and *k* is the pump constant. For variable-speed pumps and fans, the power is a function of the rotational speed per the affinity laws as shown in (8)-(10), and the motor and variable speed drive (VSD) efficiency:

$$P_{t}^{sp} = \sum\nolimits_{s \in \mathscr{S}} k_{s}^{sp} \frac{\left(VSD_{t}^{sp}\right)^{3}}{\eta_{t}^{m,sp} \eta_{t}^{VSD,sp}} \tag{8}$$

$$P_{t}^{cf} = k^{cf} \frac{\left(VSD_{t}^{cf}\right)^{3}}{\eta_{t}^{m,cf} \eta_{t}^{VSD,cf}} \tag{9}$$

$$P_{t,n}^{twr} = k_{n}^{twr} \frac{\left(VSD_{t}^{twr}\right)^{3}}{\eta_{t}^{m,twr} \eta_{t}^{VSD,twr}} ON_{t,n}^{twr} \tag{10}$$

Superscript *sp* refers to secondary pumps, *cf* refers to the coil fan, and *twr* refers to the cooling towers. $ON_{t,n}^{twr}$ are binary decision variables for the cooling tower power switch, and *VSD* is the non-dimensional rotational speed defined as the actual angular speed normalized by the maximum angular speed. The subscript n is the cooling towers index set $\{1, 2\}$ denoted by $\mathscr{N}$, and the subscript s is the secondary pumps index set $\{1, 2\}$ denoted by $\mathscr{S}$. Individual variable speed cooling tower fans and secondary pumps are identical and controlled at the same speed. For systems with a more sophisticated secondary pumping configuration, their optimal scheduling and speed configuration can be determined beforehand and represented as a function of flowrate. The optimal scheduling and speed configuration does not depend on chillers' settings upstream. Assumed pumps and fan constant values can be found in Table 4 in the Appendix. The motor and variable speed drive efficiencies as a function of their speed are obtained from correlations by Bernier and Bernard [39]:

$$\eta^{m}(VSD) = 0.94187[1 - exp(-9.04VSD)] \tag{11}$$

$$\eta^{VSD}(VSD) = \frac{1}{100}\left[50.87 + 128.3VSD - 142VSD^{2} + 58.34VSD^{3}\right] \tag{12}$$

2.1.3. Cooling towers

Cooling towers reject the heat from the condenser into the atmosphere primarily by evaporative cooling. A simple and widely used NTU-effectiveness model developed by Braun et al. [40] allows for predicting the heat rejected by the tower given air and water mass flowrates and temperatures. Although it is responsible for most of the cooling, mass transfer accounts for less than 2 % of the total water flowrate and is not factored for in the model. The fan is the sole power-consuming device. Operating cooling towers are controlled at the same speed to maintain the condenser water temperature setpoint. The NTU correlation for the cooling tower:

$$NTU_{t} = c\left(\frac{\dot{m}_{t}^{bcw} / \sum_{n \in \mathscr{N}} ON_{t,n}^{twr}}{VSD_{t}^{twr} \dot{m}^{twra,des}}\right)^{1+\varkappa} \tag{13}$$

where c and $\varkappa$ are constants for a given tower type, $\dot{m}^{twra,des}$ is the design tower air flowrate, and $\dot{m}_{t}^{bcw} / \sum_{n \in \mathscr{N}} ON_{t,n}^{twr}$ is the condenser water flowrate through each operating tower. The term $VSD_{t}^{twr} \dot{m}^{twra,des}$ is the actual mass flowrate of air through the tower, which linearly varies with fan speed per the affinity laws. The effectiveness of a counter-flow cooling tower:

$$\varepsilon_{t}^{twr} = \frac{1 - exp(-NTU_{t}(1 - C_{t}^{r}))}{1 - C_{t}^{r} exp(-NTU_{t}(1 - C_{t}^{r}))} \tag{14}$$

where,

$$C_{t}^{r} = \frac{VSD_{t}^{twr} \dot{m}^{twra,des}}{\dot{m}_{t}^{bcw} / \sum_{n \in \mathscr{N}} ON_{t,n}^{twr} \left(\frac{c^{p,cw}}{c_{t}^{s}}\right)} \tag{15}$$

$$c_{t}^{s} = \frac{h_{t}^{sat,bcrw} - h_{t}^{sat,bcsw}}{T_{t}^{bcrw} - T_{t}^{bcsw}} \tag{16}$$

$c^{p,cw}$ is condenser water-specific heat, T_{t}^{bcsw} and T_{t}^{bcrw} are chillers condenser blended entering and leaving water temperatures, respectively, $h_{t}^{sat,bcrw}$ and $h_{t}^{sat,cbsw}$ are the enthalpy of saturated air at blended leaving and entering condenser water temperatures, respectively. The effectiveness can then be used to calculate the actual heat transfer for operating cooling towers:

$$\dot{Q}_{t,n}^{twr} = VSD_{t}^{twr} \dot{m}^{twra,des} \varepsilon_{t}^{twr} \left(h_{t}^{sat,bcrw} - h_{t}^{sat,wb}\right) ON_{t,n}^{twr} \tag{17}$$

$h_t^{sat,wb}$ is the enthalpy of saturated air at the ambient wet-bulb temperatures. The considered tower characteristics are in Table 5 in the Appendix.

2.1.4. Cooling & dehumidifying coils

Sensible and latent heat from the cooled space is transferred to the chilled water in the coils by air. Coils maintain indoor comfort levels by regulating air and water flowrates. In this work, a single cooling coil representative of the entire building is modeled. The intention is to capture the complex interaction between the chillers' temperature setpoints and the required air and water flowrates and, thus, the power required in the coils to satisfy the building load. In this work, the coil is controlled to deliver the design supply air conditions, ensuring that indoor comfort is always maintained. However, information about occupancy and air distribution can be used to control cooled-space humidity and temperature more efficiently. The coil model used in this work employs expressions derived by Wang et al. for the overall heat transfer coefficient [41]:

$$NTU_t^{ext} = \frac{1}{VSD_t^{cf}\dot{m}^{cca,des}c^{p,a}} \frac{N^{row}A^{face}}{a_1^{cc}\left(VSD_t^{cf}V^{a,des}\right)^{-0.8} + a_3^{cc}} \tag{18}$$

$$NTU_t^{int} = \frac{1}{VSD_t^{sp}\dot{m}_t^{bsw}c^{p,sw}} \frac{N^{row}A^{face}}{a_2^{cc}\left(VSD_t^{sp}V^{w,des}\right)^{-0.8}} \tag{19}$$

The denominators of the two expressions are based on Holmes developed coil's thermal resistance model as a function of fluids face velocities [42]. a_1^{cc}, a_2^{cc}, and a_3^{cc} are experimentally obtained set of coefficients in Holmes's model, $\dot{m}^{cca,des}$ is the design coil air flowrate, $VSD_t^{sp}\dot{m}_t^{bsw}$ is the coil actual water flowrate, which linearly varies with speed per the affinity laws, $V^{a,des}$ and $V^{w,des}$ are the design coil air and water face velocities, respectively, $c^{p,a}$ is air specific heat capacity, A^{face} is the coil face area, and N^{row} are the number of rows or passes. The air inlet conditions can be calculated from the known exit conditions and cooling demand:

$$h^{ai} = min\left[h^{ae,des} + \frac{\dot{Q}_t^{\mathscr{D}}}{VSD_t^{cf}\dot{m}^{cca,des}}, h^{ai,des}\right] \tag{20}$$

$$T_t^{ai} = T^{ae,des} + \frac{\dot{Q}_t^{s}}{VSD_t^{cf}\dot{m}^{cca,des}c^{p,a}} \tag{21}$$

$\dot{Q}_t^{\mathscr{D}}$ is the total cooling load, $\dot{Q}_t^{s}$ is the sensible cooling load, $h^{ai,des}$ and $h^{ae,des}$ are the enthalpy of air at the coil inlet and exit under design conditions, respectively, and $T^{ae,des}$ is the coil design exit temperature. The conditions at the dry to wet transition point can be calculated from the known air and water boundary conditions:

$$h_t^{x} = h_t^{ai} - c^{p,a}\left(T_t^{ai} - T_t^{dp}\right) \tag{22}$$

$$T_t^{w,x} = \left(\frac{VSD_t^{cf}}{VSD_t^{sp}}\right)\frac{\dot{m}^{cca,des}}{\dot{m}_t^{bsw}c^{p,sw}}\left[h_t^{ai} - h^{ae,des} - c^{p,a}\left(T_t^{ai} - T_t^{dp}\right)\right] + T_t^{ccsw} \tag{23}$$

T_t^{ccsw} is the coil entering water temperature and T_t^{dp} is the dew-point temperature. The superscript x represents the point of intersection between dry and wet sections. The air temperature at the dry to wet transition is the dew point temperature and is computed from known parameters. For the dry and wet section analysis, we use Braun et al. [40] models for fully dry and fully wet coil based on the NTU-effectiveness approach. In Braun's model, the coil is modeled as a counter-flow heat exchanger since the performance of a cross-flow heat exchanger approaches that of a counter-flow when the number of passes increases beyond approximately-four. The NTU and effectiveness for the dry section are as follow:

$$NTU_t^{dry} = \frac{1}{C_t - 1} ln\left(\frac{\varepsilon_t^{dry} - 1}{C_t\varepsilon_t^{dry} - 1}\right) \tag{24}$$

$$\varepsilon_t^{dry} = \frac{T_t^{ai} - T_t^{dp}}{T_t^{ai} - T_t^{w,x}} \tag{25}$$

where,

$$C_t = \left(\frac{VSD_t^{cf}}{VSD_t^{sp}}\right)\frac{\dot{m}^{cca,des}c^{p,a}}{\dot{m}_t^{bsw}c^{p,sw}} \tag{26}$$

We then compute the exit water temperature and the fraction of the coil length in the dry section from:

$$T_t^{ccrw} = T_t^{w,x} + C_t\left(T_t^{ai} - T_t^{dp}\right) \tag{27}$$

$$f_t^{dry} = \frac{NTU_t^{dry}}{NTU_t^{ext}}\left(1 + C_t\frac{NTU_t^{ext}}{NTU_t^{int}}\right) \tag{28}$$

The NTU and effectiveness for the wet section are as follow:

$$NTU_t^{wet} = \frac{NTU_t^{ext}}{1 + m_t\left(\frac{NTU_t^{ext}}{NTU_t^{int}}\right)}\left(1 - f_t^{dry}\right) \tag{29}$$

$$\varepsilon_t^{wet} = \frac{1 - exp\left(-NTU_t^{wet}(1 - m_t)\right)}{1 - m_t exp\left(-NTU_t^{wet}(1 - m_t)\right)} \tag{30}$$

where,

$$m_t = \left(\frac{VSD_t^{cf}}{VSD_t^{sp}}\right)\frac{\dot{m}^{cca,des}}{\dot{m}_t^{bsw}c^{p,sw}}\left(\frac{h_t^{sat,ccrw} - h_t^{sat,ccsw}}{T_t^{w,x} - T_t^{ccsw}}\right) \tag{31}$$

$h_t^{sat,ccsw}$ and $h_t^{sat,ccrw}$ are the enthalpy of saturated air at coil supply and return water temperatures, respectively. We can then calculate the actual air exit enthalpy:

$$h_t^{ae} = h_t^{x} - \varepsilon_t^{wet}\left(h_t^{x} - h_t^{sat,ccsw}\right) \tag{32}$$

A feasible solution necessitates that $h_t^{ae} \equiv h^{ae,des}$. Assumed cooling coil parameters are in Table 6 in the Appendix.

2.1.5. Ice thermal storage

Ice storage stores thermal energy mainly in the form of latent heat. There are two main types of ice thermal storage, internal and external melt [43]. Unlike external melt, internal melt is modularized ice storage with predictable charge and discharge behavior. In internal melt, a secondary water-glycol mixture is circulated through an inner circuit to freeze or melt the water inside the tank. In external melt, ice comes into direct contact with supply water, delivering a rapid discharge rate suitable for specific applications. The earliest internal melt ice storage model appears to be developed by Jekel [44] and was later improved by Drees [45,46]. We use the model improved by Drees with specifications based on a product of CALMAC with 83 ton-hr nominal capacity. Twenty tanks are balanced and joined in parallel, which acts as a single ice tank with an equivalent thermal capacity of 1600 ton-hr. Control of the ice bank is accomplished by regulating the inlet temperature and flowrate as described by the heat balance equation:

$$\dot{m}_t^{isw} c^{p,sw}\left(T_t^{isw} - T_t^{bsw}\right) = \dot{H} = h^{sf}\dot{m}_t^{is,ice} - m_t^{is,tank} c^{p,w}\dot{T}_t^{is} \tag{33}$$

$\dot{m}_t^{isw}$ is the circulating water-glycol mix flowrate, T_t^{isw} is the water-glycol mixture temperature at the outlet of the storage tank, and T_t^{is} is the average storage temperature. $\dot{m}_t^{isw} c^{p,sw}\left(T_t^{isw} - T_t^{bsw}\right)$ is the rate of heat transfer to the circulating water-glycol mixture, $\dot{m}_t^{is,ice}$ is the rate of ice formation, h^{sf} is the enthalpy of fusion of water, and $m_t^{is,tank}$ is the total mass of water in the tank, sensible heat of water, $\dot{T}_t^{is}$ is the rate of change of the average temperature of the tank, $c^{p,w}$ is the specific heat of tank water. Sensible heat change of ice can be neglected because of the reduced thermal capacity of ice relative to water and the smaller temperature difference between ice and the freezing point of water. The rate of change of enthalpy can also be obtained from the LMTD method which is given by:

$$\dot{H} = \left(\frac{1}{R_t^{int} + R_t^{ext}}\right)\left[\frac{T_t^{isw} - T_t^{bsw}}{ln\left(\frac{T_t^{is} - T_t^{isw}}{T_t^{is} - T_t^{bsw}}\right)}\right] \tag{34}$$

The external thermal resistance term R_t^{ext} depends on both the mode of operation, charging or discharging, and the state of charge; both R_t^{int} and R_t^{ext} are obtained from Drees's model [45,46]. Heat loss through tank walls is ignored since they are well insulated with a self-discharge efficiency of 99.9% [47]. The charging of ice storage is divided into three stages, as shown in Fig. 3: sensible, unconstrained phase change, and area-constrained phase change. In sensible charging, the water temperature in the tank is brought down to freezing temperature without ice formation. Upon reaching freezing temperature, unconstrained phase change initiates with uniform cylindrical ice formation around the tubes. Once the ice formations intersect, heat transfer becomes increasingly area constrained until all the water around the tubes is frozen. Similarly, discharging of ice storage is divided into three stages, also shown in Fig. 3: unconstrained phase change, area-constrained phase change, and sensible. In the first stage, the ice closest to the tube is melted. The water-glycol mixture passing through the tubes is cooled down at the expense of 1) warming a layer of liquid water between the outer surface of the tube and the water–ice interface and 2) a receding liquid water–ice interface. When the ice-liquid water interfaces intersect, heat transfer reduces due to the reduced surface area of ice formations. Once all ice has melted, the storage water temperature is gradually brought to the circulating water temperature. For this and all subsequent figures, cooling demand is shown in tons or Ton (Ton of Refrigeration).

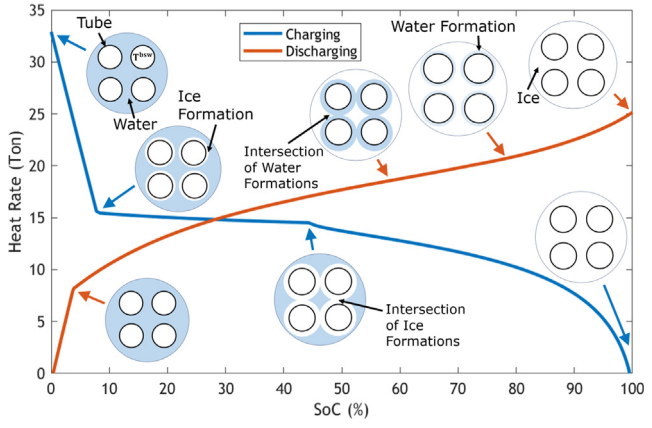

Fig. 3. An illustration of the charging and discharging process in a cross-sectional view of an 80 ton-hr internal melt ice storage tank is shown along the heat rate curve. The intersection of ice formations when charging and water formations when discharging reduces the heat transfer area. Charging is at −6 °C 4 kg/s, and discharging at 8 °C 4 kg/s.

Drees shows that the effectiveness defined as the ratio of actual to the maximum temperature difference is insensitive to inlet temperature but is a strong function of flow rate and state of charge. This is used to reduce the storage model to a function of flow rate and stage of charge. The storage effectiveness is defined as:

$$\varepsilon^{is} = \frac{T^{bsw} - T^{isw}}{T^{bsw} - T^{is}} \tag{35}$$

A 2-D effectiveness surface is generated from the simulation of full storage charge and discharge cycles at multiple increments of flow rates and linearly interpolated for all flowrates in-between to obtain a function of the form:

$$\varepsilon_t^{is} = f\left(SoC_t, \dot{m}_t^{isw}, sgn(SoC_{t+1} - SoC_t)\right) \tag{36}$$

SoC_t is the storage state of charge. The 2-D surface is indexed by three parameters: the state of charge, the inlet flowrate, and mode (charging/discharging). Equation (35) is re-arranged to compute the storage outlet temperature as follows:

$$T_t^{isw} = T_t^{bsw} - \varepsilon_t^{is}(T_t^{bsw} - T_t^{is}) \tag{37}$$

The state of charge is updated for the next time step as follows:

$$SoC_{t+1} = SoC_t + \frac{\dot{m}_t^{isw} c^{p,sw}\left(T_t^{isw} - T_t^{bsw}\right)}{C^{is}}\Delta t \tag{38}$$

C^{is} is ice storage thermal capacity and Δt is the time step in seconds. The storage effectiveness, ε_t^{is}, is updated in increments of 10 min to factor in any change in charge and discharge rates within a time step. Simulation of ice storage operation under different water flowrates and inlet temperatures are shown in Fig. 4 (A) and (B) for charging and Fig. 4 (C) and (D) for discharging. Note that the difference in effectiveness due to inlet temperature is negligible. Furthermore, daily storage operation requires an inlet temperature close to −6°Cwhich can significantly depress chiller performance and cooling capacity.

2.2. Overall problem formulation

The overall framework is to determine the scheduling of equipment, setpoints, and storage dispatch amount such that the cooling load is met with the least cost. This is influenced by the cooling load, storage capacity and utilization, and TOU rates. The models developed for each key power-consuming component appear in the overall formulation with several operational and balancing constraints. The cost which is to be minimized is given by $\sum_t c_t^e P_t^{Sys}$, where:

$$P_t^{Sys} = \sum_{i\in\mathcal{I}}\left(P_{t,i}^{chl} + P_{t,i}^{pp} + P_{t,i}^{cp}\right) + \sum_{n\in\mathcal{N}} P_{t,n}^{twr} + P_t^{sp} + P_t^{cf} \tag{39}$$

c_t^e is TOU rate at time step t, and P_t^{Sys} is total system power use at time step t. The first constraint bounds operating chillers to within permitted load ratios:

$$PLR_i^{min} \le PLR_{t,i} \le PLR_{t,i}^{max} \tag{40}$$

where $PLR_{t,i} = \dot{Q}_{t,i}^{chl}/\dot{Q}_i^{des}$. PLR_i^{min} is the minimum chillers operating part load ratio obtained from EnergyPlus and $PLR_{t,i}^{max} = \dot{Q}_{t,i}^{max}/\dot{Q}_i^{des}$ is from the estimated chiller cooling capacity. The second and third constraints bound and set the initial storage state of charge:

$$0 \le SoC_t \le 1 \tag{41}$$

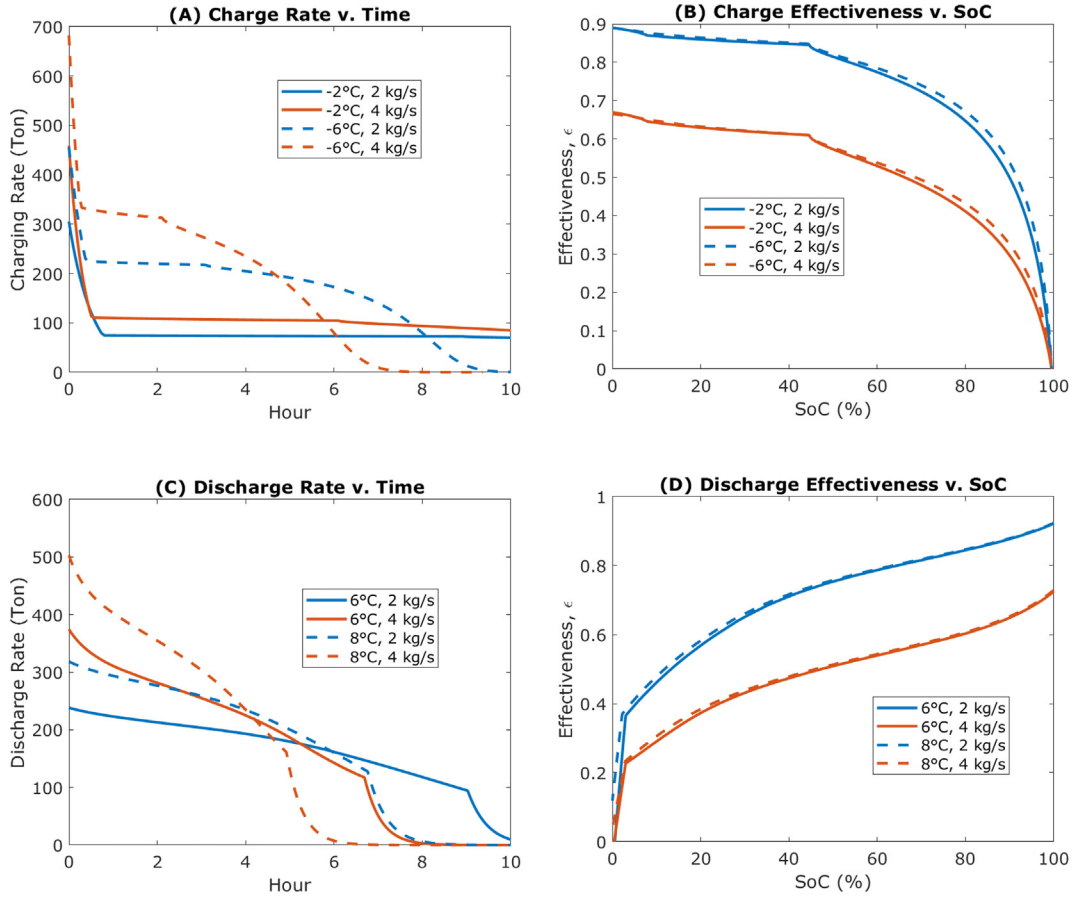

Fig. 4. Simulation of ice storage operation under different inlet conditions for charge mode with (A) charging rate and (B) charging effectiveness, and discharge mode with (C) discharge rate and (D) discharging effectiveness. Storage is fully charged at an SoC of 100 and fully discharged at an SoC of 0.

$$SoC_0 = 0 \tag{42}$$

The fourth constraint bounds the fraction of the coil in the dry section:

$$0 \leq f_t^{dry} \leq 1 \tag{43}$$

Constraints five to seven are three load balancing constraints:

$$\sum_{i\in\mathscr{I}} \left(PLR_{t,i}\dot{Q}_i^{des}\right) - \dot{m}_t^{isw} c^{p,sw}\left(T_t^{isw} - T_t^{bsw}\right) - \dot{Q}_t^{\mathscr{D}} = 0 \tag{44}$$

$$VSD_t^{sp}\dot{m}_t^{bsw} c^{p,sw}\left(T_t^{ccrw} - T_t^{ccsw}\right) - \dot{Q}_t^{\mathscr{D}} = 0 \tag{45}$$

$$VSD_t^{cf}\dot{m}^{cca,des}\left(h_t^{ai} - h_t^{ae}\right) - \dot{Q}_t^{\mathscr{D}} = 0 \tag{46}$$

The constraints ensure the building demand, $\dot{Q}_t^{\mathscr{D}}$, is met by the chiller and storage in (44) and delivered to the coil in the water-side in (45) and the air side in (46). The fourth balancing constraint balances mass flowrate to storage and available mass flowrate in the primary loop whic is given by:

$$\dot{m}_t^{bsw} - \dot{m}_t^{isw} \geq 0 \tag{47}$$

The final and fifth balancing constraint balances the heat rejected by the chillers and cooling towers as follows:

$$\dot{m}_t^{bcw} c^{p,cw}\left(T_t^{bcrw} - T_t^{bcsw}\right) - \sum_{n\in\mathscr{N}} \dot{Q}_{t,n}^{twr} ON_{t,n}^{twr} = 0 \tag{48}$$

The decision variables are: chillers and tower scheduling ($ON_{t,i}^{chl}$ and $ON_{t,n}^{twr}$), chillers temperatures setpoints ($T_{t,i}^{sw}$), towers temperature setpoints and speed (T_t^{bcsw} and VSD_t^{twr}), coil fan and pump speeds (VSD_t^{sp} and VSD_t^{cf}), and flowrate to storage ($\dot{m}_t^{isw}$).

Designated temperatures and flowrates symbols at various system nodes that appear in the problem formulation are shown in Fig. 5. The total flowrates in the primary and condenser loops are dependent on the design evaporator and condenser flowrates, respectively, for operating chillers, which are given by:

$$\dot{m}_t^{bsw} = \sum_{i\in\mathscr{I}} \dot{m}_i^{sw} ON_{t,i}^{chl} \tag{49}$$

$$\dot{m}_t^{bcw} = \sum_{i\in\mathscr{I}} \dot{m}_i^{cw} ON_{t,i}^{chl} \tag{50}$$

Primary loop blended supply and return temperature are calculated from the mixing of streams as follows:

$$T_t^{bsw} = \sum_{i\in\mathscr{I}} \frac{\dot{m}_i^{sw}}{\dot{m}_t^{bsw}} T_{t,i}^{sw} ON_{t,i}^{chl} \tag{51}$$

$$T_t^{brw} = VSD_t^{sp} T_t^{ccrw} + \left(1 - VSD_t^{sp}\right) T_t^{ccsw} \tag{52}$$

The water-glycol mixture temperature at the coil inlet deviates from the blended supply water temperature based on the storage dispatch amount:

$$T_t^{ccsw} = \left(1 - \frac{\dot{m}_t^{isw}}{\dot{m}_t^{bsw}}\right) T_t^{bsw} + \frac{\dot{m}_t^{isw}}{\dot{m}_t^{bsw}} T_t^{isw} \tag{53}$$

The temperature of the blended condenser water that is returning to the cooling tower is:

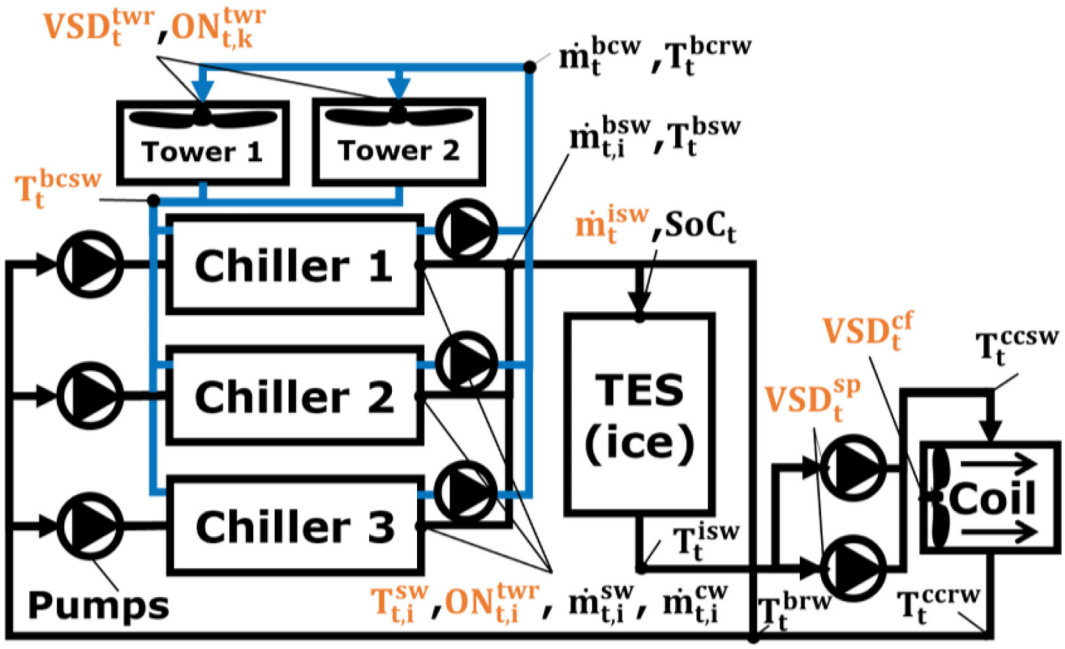

Fig. 5. Considered chilled water system with ice thermal storage. Highlighted variables in orange are the decision variables; variables in black are consequences of the decision variables. (For interpretation of the references to colour in this figure legend, the reader is referred to the web version of this article.)

$$T_t^{bcrw} = T_t^{bcsw} + \frac{\sum_{i\in\mathscr{I}}\left(P_{t,i}^{chl} + \dot{Q}_{t,i}^{chl}\right)}{\dot{m}_t^{bcw} c^{p,cw}} \tag{54}$$

A water-glycol mixture is considered in the primary and the secondary loop to allow safe operation at sub-freezing temperatures. The thermal capacity of the mixture is depressed by about 10 % relative to pure water.

2.3. Optimization strategy

2.3.1. Bi-level optimization

Because of the nonlinearity and the large number of degrees of freedom, the problem described above cannot be reliably solved using traditional gradient-based or *meta*-heuristic optimization strategies. As illustrated in Fig. 6, the solution approach is to decompose the problem into a bi-level optimization formulation to decouple the equipment scheduling problem at each hour from storage dispatch. This simplifies the scheduling problem sufficiently to allow for the use of the genetic algorithm for both levels. The upper level minimizes daily operation costs and decides the storage dispatch amount over the next 24 h. The decided dispatch amount is fed to the lower-level optimizer to solve the equipment scheduling problem at each hour sequentially and return the corresponding system power consumption over the next 24 h. The lower-level problem is constrained by six load and flowrate balancing constraints; the added sixth constraint ensures that the dispatched amount in the lower level agrees with the decided dispatch amount by the upper-level optimizer. The balancing constraints are handled using the penalty function method. Storage dispatch amounts decided by the upper-level optimizer that lead to infeasible solutions are penalized. The bi-level objective functions are:

$$minObj^1 = \sum_{t\in\mathscr{T}} c_t^e P_t^{Sys} \tag{55}$$

$$minObj_t^2 = \left(P_t^{Sys}/P^{Sys,des}\right)^{\alpha} + \mathbb{C}_t, \tag{56}$$

$$\mathbb{C}_t = \begin{bmatrix} a_1\left|1 - \frac{\dot{m}_t^{isw} c^{p,sw}\left(T_t^{isw} - T_t^{bsw}\right) + \dot{Q}_t^{\mathscr{D}}}{\sum_{i\in\mathscr{I}}\left(PLR_{t,i}\dot{Q}_t^{des}\right)}\right|^{b_1} \\ +a_2\left|\frac{VSD_t^{sp}\dot{m}_t^{bsw} c^{p,sw}\left(T_t^{ccrw} - T_t^{ccsw}\right) + \Delta}{\dot{Q}_t^{\mathscr{D}} + \Delta} - 1\right|^{b_2} \\ +a_3\left|\frac{VSD_t^{cf}\dot{m}^{cca,des}\left(h_t^{ai} - h_t^{ae}\right) + \Delta}{\dot{Q}_t^{\mathscr{D}} + \Delta} - 1\right|^{b_3} \\ +a_4\left|1 - \frac{\dot{m}_t^{isw}}{\dot{m}_t^{bsw}}\right|^{b_4}\left[\dot{m}_t^{isw} > \dot{m}_t^{bsw}\right] \\ +a_5\left|\frac{\dot{m}_t^{bcw} c^{p,cw}\left(T_t^{bcrw} - T_t^{bcsw}\right)}{\sum_{n\in\mathscr{N}}\dot{Q}_{t,n}^{twr} ON_{t,n}^{twr}} - 1\right|^{b_5} \\ +a_6\left|SoC_t - SoC_t^{ulo}\right|^{b_6} \end{bmatrix} \tag{57}$$

where α, a_1 to a_6, and b_1 to b_6 are the penalty factors, and SoC_t^{ulo} is the storage dispatch amount decided by the upper-level, and Δ is an arbitrary small load (less than1% of $\dot{Q}^{des}$) with the same unit as $\dot{Q}_t^{\mathscr{D}}$. Bound constraints on chillers part load ratio and storage state of charge in (40)-(41) are enforced by resetting the violating variable to the nearest bound. This inevitably leads to violation of balancing constraints and thus discourages the genetic algorithm from exploring that search space area. Solutions that violate the bound constraint in (43) cannot be truncated and are better when eliminated from the gene pool in the genetic algorithm.

Constraints are relaxed to allow for a violation of no more than 3 %, although they largely fall far below 1 %. The system power use over the next 24 h, as determined by the lower-level optimizer, is returned to the upper-level optimizer to update the storage dispatch guess for the next iteration. The inputs for the upper level are the TOU electricity prices, and the inputs for the lower level are the cooling load (sensible and latent), ambient wet-bulb temperature, and storage state of charge at the end of the previous time step. The decision variable for the upper-level problem is the storage dispatch amount (ΔSoC_t) and the decision variables for the lower-level problem are setpoints ($T_{t,i}^{sw}, T_t^{bcsw}, \dot{m}_t^{isw}, VSD_t^{cf}, VSD_t^{sp}, VSD_t^{twr}$) and equipment scheduling

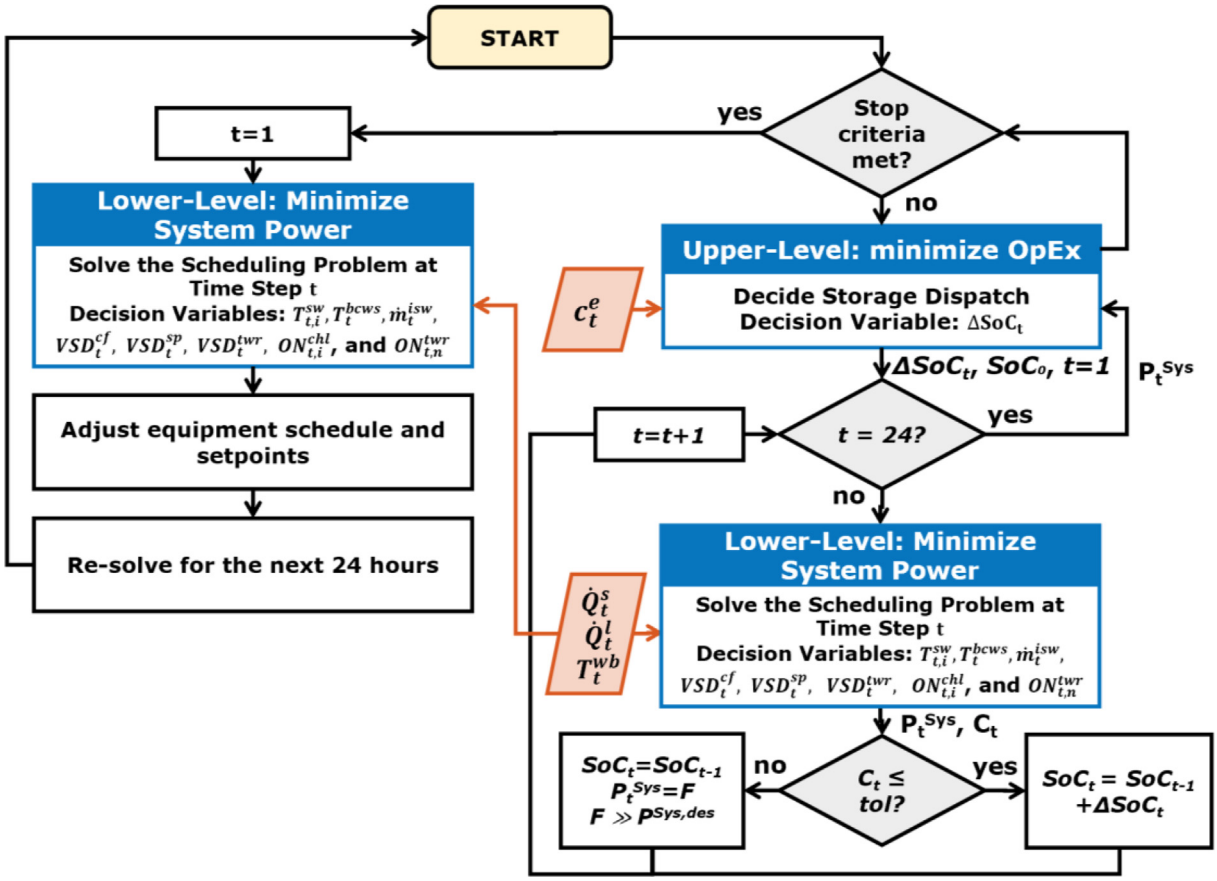

Fig. 6. Bi-level optimization strategy. the upper decided dispatch is passed down to the lower-level optimizer to solve the equipment scheduling problem sequentially. Infeasible storage dispatch at a given hour is rejected and penalized. The upper-level optimizer input is the TOU tariff, and lower-level optimizer inputs are the sensible and latent cooling load and ambient wet-bulb temperature. The genetic algorithm is applied to both levels.

($ON_{t,i}^{chl}$, and $ON_{t,n}^{twr}$). The converged storage dispatch amount curve (ΔSoC v. time) is used to adjust equipment sequencing and setpoints at the current time step before re-solving for the next 24 h.

2.3.2. Parameters tuning

Balancing constraints in the lower-level problem are handled using the penalty function method; this makes the objective function subject to influence by both the system power use as well as violations of balancing constraints. This poses a challenge for the genetic algorithm to assess the population's fitness effectively. There are 13 penalty factors in (56)-(57); manual tuning of the 13 penalty factors is difficult and cumbersome, especially considering the impact of the cooling load, ambient wet-bulb temperature, and storage use on the solution space. In addition to penalty factors, genetic algorithm parameters such as population size, crossover rate, number of generations, number of stall iterations, and elite count, among others, can highly impact the quality of the converged solution. A more systematic and robust approach is to tune the penalty factors and genetic algorithm parameters with a training dataset using an optimizer for which we use particle swarm optimization.

Training data are manufactured by sampling various possible operating combinations of cooling load, ambient wet-bulb temperature, and storage state of charge and dispatch amount. Feasible solutions, irrespective of optimality, should satisfy the constraints and hence can be used to tune the penalty factors. The intention is to allow the genetic algorithm to distinguish apart the contribution of each variable to the objective function, better assess the population fitness and locate a feasible, globally optimal solution. The considered manufactured training data are shown in Fig. 7; the dataset contains 237 unique combinations of possible cooling demand, ambient wet-bulb temperature, storage dispatch amount, and storage state of charge. The objective function for the penalty factor tuning optimization is:

$$minObj = \sum_{z \in \mathscr{Z}} [P_z + \beta \mathbb{C}_z] \tag{58}$$

and,

$$P_z = \begin{cases} P_z^{Sys} & \mathbb{C}_z \leq tol \\ F & Otherwise \end{cases} \tag{59}$$

where subscript z is data point index set {1, 2, 3, …, 237} denoted by $\mathscr{Z}$ and β is manually adjusted constant such that $\beta \mathbb{C}_z$ sufficiently reduces constraints violation but not large enough to meaningfully impact the objective function, tol is the constraint relaxation tolerance (taken as 3 % in this study), and F penalizes ($F \gg P^{Sys,des}$) infeasible solutions (C_z > tol) Proper tuning of the penalty factors can significantly diminish and eliminate the problem of premature convergence in the genetic algorithm. The optimal system COP for three modes of storage operation (charging, discharging, and idle) generated for the considered system under a range of cooling loads are shown in Fig. 8 at a design wet-bulb temperature of 25 °C Despite the high nonlinearity and complexity of the considered problem, the tuned penalty factor and genetic algorithm parameters resulted in near-smooth and continuous system

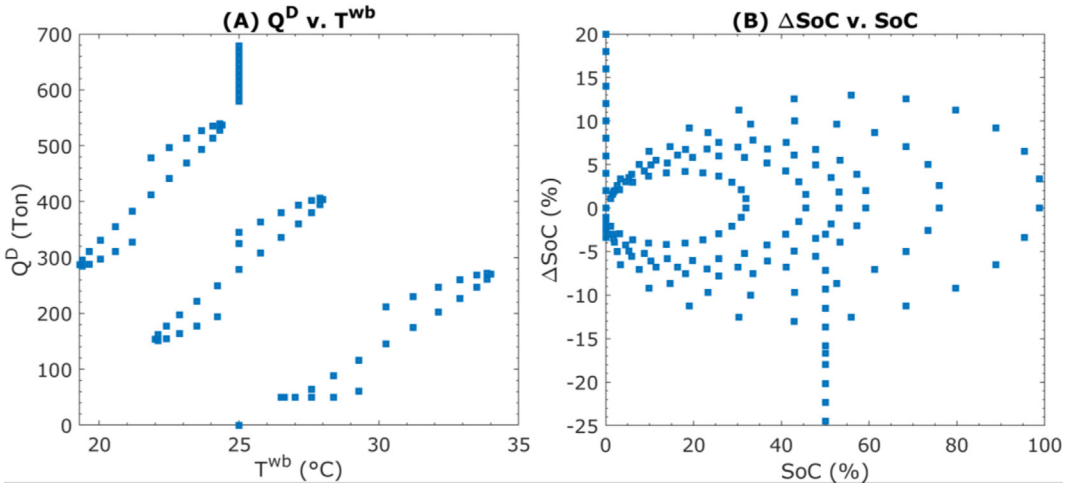

Fig. 7. Training data. (A) Cooling demand and ambient wet-bulb temperature, and (B) Storage dispatch amount and state of charge. This training set has 237 unique data points, each an independent input condition for the scheduling problem. A sensible heat ratio of 0.7 is assumed for the cooling load.

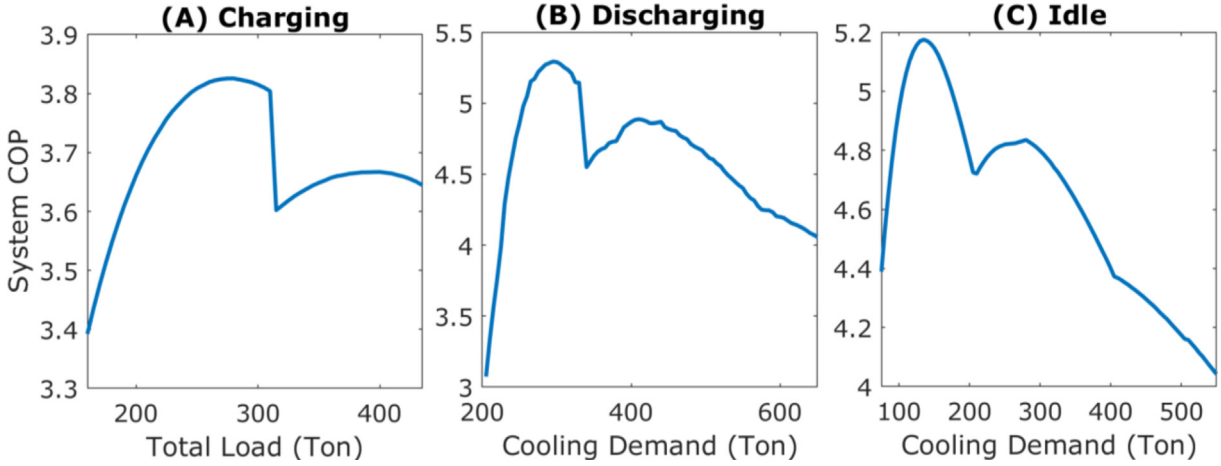

Fig. 8. System COP for a range of cooling loads at a wet-bulb temperature of 25 °C when (A) charging at a rate of 160 ton-hr/hr, (B) discharging at a rate of 160 ton-hr/hr, and (C) not using ice storage. The total load includes the cooling load and the storage charge amount.

performance curves. The curve's shape is a consequence of the three chillers system. There are two configurations for operating this system when charging at a rate of 160 tons in Fig. 8 (A) since the smallest chiller cannot provide sufficient cooling on its own. At a total load lower than 300 tons, the system utilizes a more efficient configuration of two centrifugal chillers for charging.When discharging or idling, like in Fig. 8 (B) and (C), the more complex shape is caused by the operation of the three chillers. At lower loads, it is sufficient to use one chiller to reduce parasitic pump energy use. However, as the load increase, more thoughtful consideration is necessary to schedule the remaining chillers. At higher loads, the system is obligated to use all chillers.

Meta-heuristic algorithms are computationally taxing as they depend on exploring the solution space to locate the globally optimal solution, especially with the large population size (1000–5000) needed to solve the highly non-linear problem at hand. To tackle the problem of long run time, the lower-level problem is pre-solved under a range of cooling loads, storage use and state, and ambient air conditions; tri-linear interpolation is applied between the data points. This reduces the run time to 1–5 min, depending on processing power, problem size, and complexity.

3. Results & discussion

We compare the proposed optimal control strategy to two popular and commonly used heuristic strategies for thermal energy storage dispatch: chiller priority control and storage priority control. In chiller priority control, chillers are loaded at capacity, and storage is used to supplement additional cooling needs. This strategy aims to maximize the efficiency of the chillers. In storage priority control, full storage capacity is utilized, and storage dispatch is prioritized over the chillers. Storage supplies a steady cooling rate, and the chillers meet the residual and fluctuating cooling demand. Storage is charged at the maximum rate the chillers allow in both heuristic strategies. For storage and chiller priority controls, the scheduling problem is solved heuristically as follows:

- 212-tons centrifugal chillers with VSD are operated first before the 153-tons screw chiller is started because of the higher efficiency
- Charging at chillers supply temperature setpoint of −7 °C
- Discharging at chillers design supply temperature setpoint of 6 °C temperature is gradually increased if necessary to maintain storage dispatch amount

- Cooling tower condenser water temperature setpoint based on design approach temperature of 3 °C (difference between leaving water and ambient air wet-bulb temperatures)
- Operating cooling tower is fully loaded before the second one is started

The three storage dispatch strategies are compared in three scenarios of cooling loads under TOU rates shown in Fig. 9. The use of ice storage becomes necessary to satisfy building cooling demand when the load exceeds the design chillers' cooling capacity of 570 tons. Scenario 1, which has the highest total cooling needs, begins at 8 AM and terminates at 6 PM. The load peaks at 600–700 tons and requires 976 ton-hr of stored energy (61 % of storage capacity) to satisfy building cooling demand. Scenario 2 has intermediate cooling needs and similarly starts at 8 AM and terminates at 6 PM. The load peaks at 550–650 tons and require 544 ton-hr of stored energy (34 % of storage capacity). Scenario 3 has the least cooling needs, starting later at 9 AM and ending earlier at 5 PM. This demand scenario peaks at 500–600 tons and requires only 144 ton-hr of stored energy (9 % of storage capacity). Simple two levels TOU tariffs are considered with an on-peak period lasting 8 h between 8 AM and 4 PM and an off-peak period otherwise. The TOU tariff doubles from $0.1/kWh in the off-peak period to $0.2/kWh in the on-peak period, coinciding with a high building cooling load. For all three scenarios, the ambient wet-bulb temperature is lower during early morning hours and higher during the evening, which overlaps with the cooling load and slightly depresses the chiller capacity.

The formulated problem is solved for the three scenarios using each of the three considered strategies, and the results are tabulated in Table 1. The hourly load contribution from each chiller and the storage to meet the cooling demand is shown in Fig. 10. The hourly system characteristics for all scenarios are shown in Fig. 11 with (A) system operation cost, (B) system total energy use, (C) chiller energy use, and (D) auxiliary equipment energy use, and in Fig. 12 with (A) system COP, (B) blended chillers evaporator leaving temperature, (C) blended chillers condenser leaving water temperature, (D) storage dispatch amount, and (E) flowrate to storage. Optimal dispatch and equipment scheduling reduce operation costs by 17 %, 19 %, and 23 %, and total energy use by 9 %, 5 %, and 1 % for Scenario 1, 2, and 3, respectively, relative to chiller priority control. Although chiller priority control attempts to maximize chillers' efficiency, the missed opportunity cost from load shifting combined with sub-optimal chiller scheduling resulted in a significantly higher system cost. Relative to storage priority control, optimal control reduces operation costs by 14 %, 11 %, and 11 %, and total energy use by 12 %, 11 %, and 11 % for Scenario 1, 2, and 3, respectively. In addition to cost reduction, the cost-optimal control system reduced daily energy use, which corresponds to carbon emissions reduction. Although auxiliary equipment energy use [shown in Fig. 11 (D)] is small and minimally impacts the overall system energy use compared to chillers' energy use [shown in Fig. 11 (C)], their interaction with the chillers significantly impacts chillers' performance and consequently their energy use.

Storage is more efficiently charged in the optimal control compared to heuristic strategies; the cost-optimal control system only utilizes the more efficient 212-tons centrifugal chillers with VSD for storage charging. Although it prolongs the charging period by an additional hour compared to storage priority control, it evades running the chillers at a reduced part-load ratio and thus increases overall efficiency. The utility from the higher flowrate provided by the third chiller is diminished by the deterioration of ice storage effectiveness. It is worth noting that the storage was not fully charged in optimal control under all considered scenarios to avoid the increased thermal resistance around the ice storage coils at the end of the charging cycle. For all strategies, storage was charged at a water-glycol mixture inlet supply temperature of −7 °C as shown in Fig. 12 (B).

In Scenario 1, the cooling demand far exceeded the design chiller capacity, which required using all three chillers. The higher efficiency attained in the optimal control is primarily due to the optimal loading of the three chillers. The model results suggested loading the screw chiller fully and equally part-loading the 212 tons VSD centrifugal chillers. As the demand is reduced in Scenario 2 and further in Scenario 3, the screw chiller is progressively displaced, and when operated, it is fully loaded. An exception is in Scenario 3 at 3 PM, where the use of a screw chiller was necessary to provide sufficient water flowrate to discharge the ice storage. Not only that, but the model also attempts to operate the VSD centrifugal chillers at their maximum efficiency point with a part load ratio between 0.8 and 0.9. This is more easily accomplished in Scenario 3 when storage dispatch is less constrained by the cooling demand.

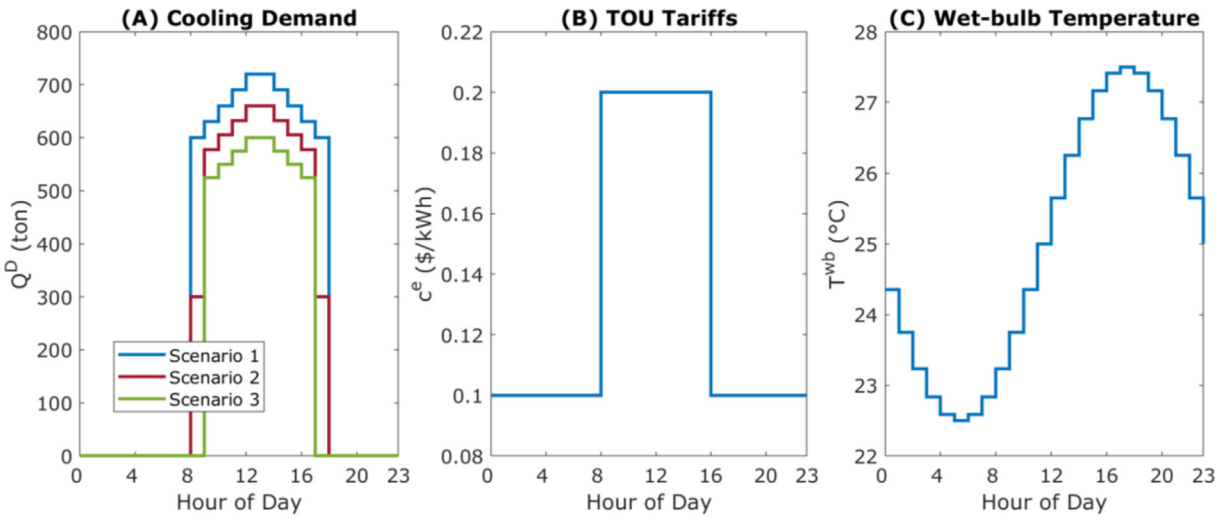

Fig. 9. Considered hourly (A) three scenarios of cooling load, (B) TOU tariffs structure, and (C) ambient wet-bulb temperature profiles. The cooling load is divided into 70% sensible and 30% latent.

Table 1
Daily cost, energy use, and storage utilization for the considered scenarios and control strategies.

	Optimization Strategy	Cost ($/day)	Energy (kWh/day)	Storage Utilization (% of Capacity)	Difference to Optimal System Cost (%)
Scenario 1	Chiller Priority Control	1070	6434	61	17
	Storage Priority Control	1045	6610	100	14
	Optimal Control	916	5888	96	–
Scenario 2	Chiller Priority Control	909	5215	34	19
	Storage Priority Control	852	5485	100	11
	Optimal Control	766	4954	96	–
Scenario 3	Chiller Priority Control	746	4068	9	23
	Storage Priority Control	675	4470	100	11
	Optimal Control	606	4013	96	–

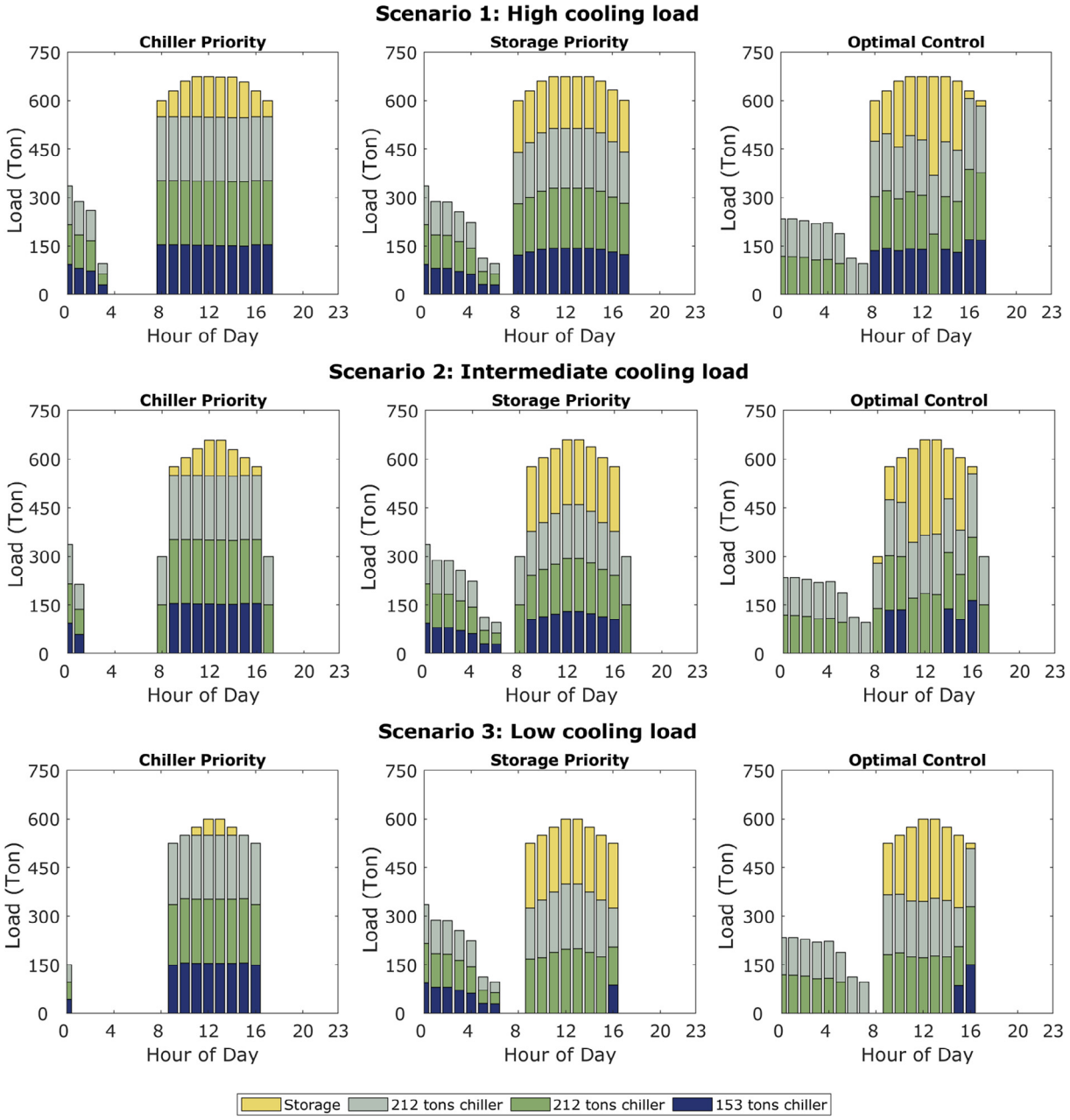

Fig. 10. Cooling demand contribution breakdown from each chiller and storage for the three control strategies. From the left to right. chiller priority control, storage priority control, and optimal storage control. The system comprises two 212-tons centrifugal chillers with VSD (Carrier 19XR) and one 153-tons screw chiller (Trane RTHB).

Supply water flowrate to ice storage is shown in Fig. 12 (E); the reduced flowrate in the optimal control strategy caused by switching off the screw chiller is traded with an increased supply temperature during discharge, enhancing system COP. Compared to heuristic strategies, discharging of storage largely terminates before the end of on-peak electricity pricing, further contributing

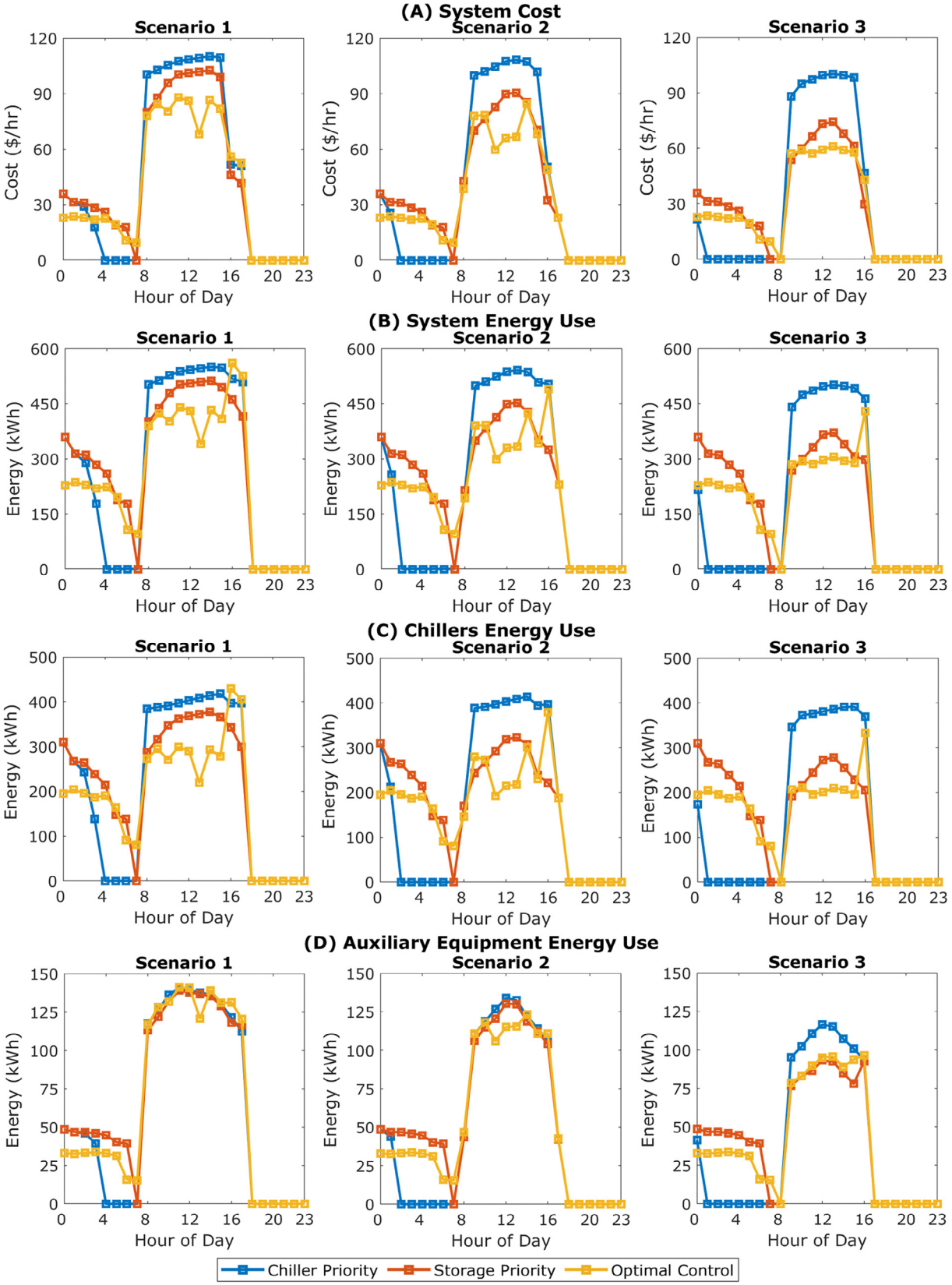

Fig. 11. For the three control strategies, hourly systems. (A) system operation cost; (B) total system electric energy use; (C) total energy use by all chillers excluding auxiliary equipment; (D) auxiliary equipment energy use which includes primary, secondary and condenser pumps, and towers and coil fans.

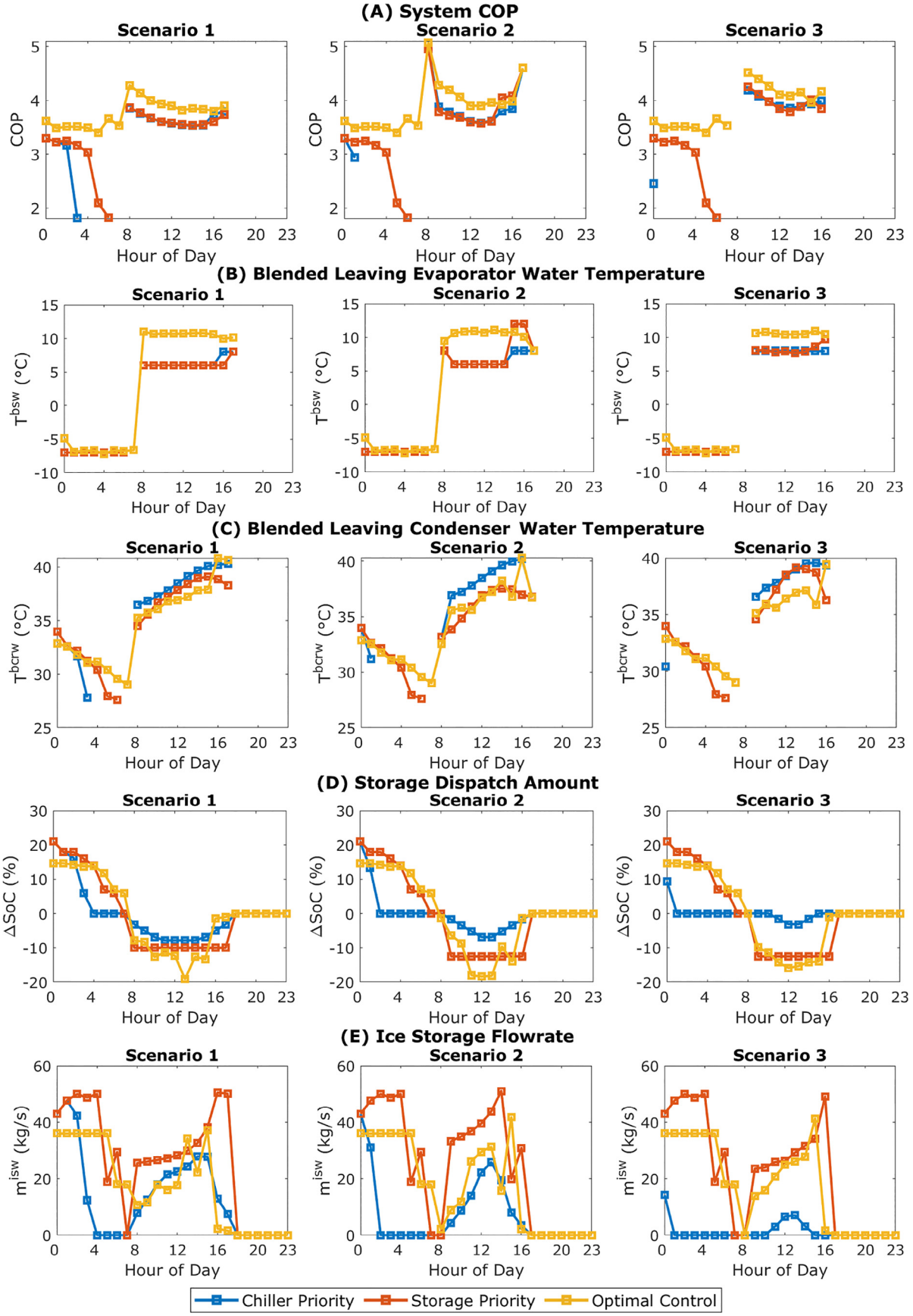

Fig. 12. For the three control strategies**,** hourly systems**.** (A) COP, (B) blended chillers supply temperature; (C) blended chillers condenser leaving water temperature; (D) storage dispatch amount curve; (E) water flowrate to ice storage. System COP is the ratio of total chillers thermal load to the overall system electric load.

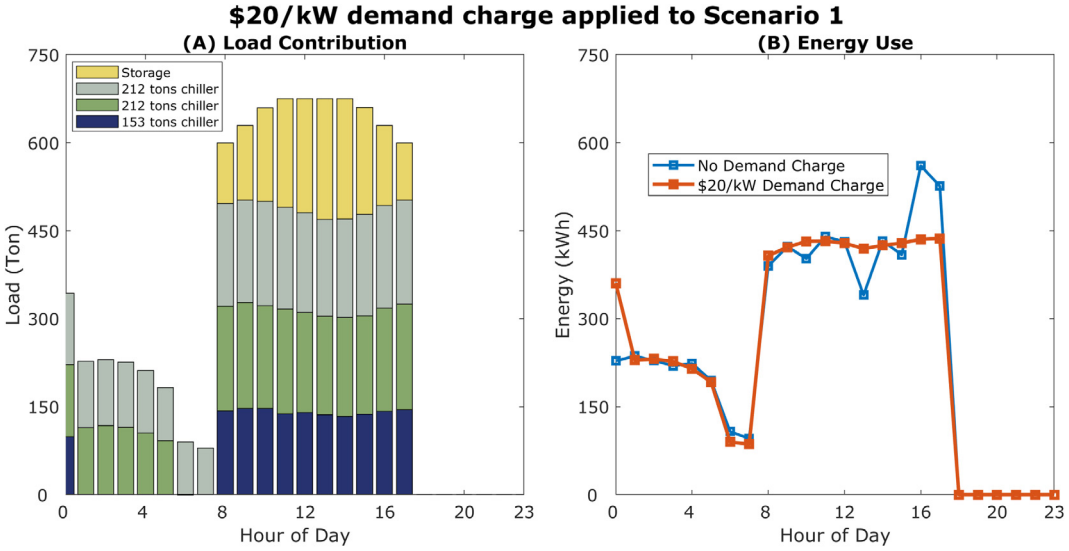

Fig. 13. Scenario 1 with a demand charge of $20/kW. (A) Breakdown of cooling demand contribution from each chiller and storage and (B) System electric energy use. We assume the demand in Scenario 1 is repeated daily for a month representing a high cooling demand season.

to cost savings. This was achieved by re-setting the water supply temperature at the outlet of the chillers above the design point by 2–3 °C which enhanced the chillers' cooling capacity, particularly the 153-tons chiller with a positive displacement screw compressor. Other sources of enhanced system COP are lower condensing temperatures, specifically during the discharging period, shown in Fig. 12 (C).

We resolved the formulated problem with the addition of a demand charge of $20/kW applied for Scenario 1, the scenario with the highest cooling demand. We make the assumption that the demand in Scenario 1 is repeated daily for a month. Our model result suggests that the cost-optimal system can reduce peak electric demand by 75 kW and cost from demand charges by 17 % relative to storage priority and 113 kW and 26 % relative to chiller priority controls. The inclusion of the demand charge results in an increase in daily cost from energy use from $916/day to $928/day. Despite the increased thermal resistance around the ice storage coils at the end of the charging cycle, the inclusion of demand charge results in the system fully utilizing the storage capacity for load shifting and peak demand reduction. Fig. 13 shows the cost-optimal system load contribution breakdown in (A) and hourly energy use in (B) when a demand charge of $20/kW is applied to Scenario 1.

4. Conclusion

Soaring demand for energy-intensive space cooling mandates a more sustainable cooling approach to reducing carbon emissions. In regions with a TOU rate, thermal energy storage can reduce required chiller cooling capacity and electricity bill charges through load shifting and peak shaving. In this paper, we propose a solution to the optimal scheduling and dispatch problem of multi-chiller chilled water systems with ice thermal storage under TOU rates. Physics-based steady-state models are considered for the ice thermal storage and the key power-consuming components, including the chillers, cooling towers, water pumps, and cooling coils. The solution strategy is to decompose the problem into bi-level optimization to decouple the equipment scheduling problem from storage dispatch, which sufficiently simplifies the problem. The genetic algorithm is used to solve the simplified problem. The upper level minimizes operation costs and decides the storage dispatch amount that is fed to the lower-level optimizer to solve the equipment scheduling problem sequentially and return the subsequent system power consumption. Constraints in the lower-level problem are handled using the penalty function method. Tuning the penalty factors and genetic algorithm parameters using an optimizer and training data diminished and eliminated the premature convergence problem. This proposed novel approach negates the need for simplistic system models for complex space cooling and heating applications.

We compared the developed optimal control strategy to two commonly used heuristic storage strategies: chiller priority control and storage priority control, in three scenarios of cooling demand under TOU tariffs. The model results suggest that the optimal control strategy consistently offered cost reduction by 17–23 % relative to chiller priority control and 11–12 % relative to storage priority control. Furthermore, optimal equipment and scheduling dispatch reduced energy use by 1–9 % relative to chiller priority and 11–12 % relative to storage priority control. When we reconsidered Scenario 1 with a demand charge of $20/kW, the optimal system can reduce peak demand power and cost from demand charge by 75 kW and 17 %, respectively, relative to storage priority and by 113 kW and 26 % relative to chiller priority controls. The benefits from the proposed strategy are amplified when a more sophisticated tariff structure is present. Lastly, at the cost of increased computational time, the proposed approach can be used to decide storage dispatch over a more extended period than 24 h.

Data availability

No data was used for the research described in the article.

Declaration of Competing Interest

The authors declare that they have no known competing financial interests or personal relationships that could have appeared to influence the work reported in this paper.

Acknowledgment

This research was sponsored by Qgrants thru Qatar National Research Fund (QNRF) with a grant number QRLP10-G-1803028.

Appendix

Table 2
Selected water chillers' characteristics

Item	Water-Cooled Chillers	
	Trane RTHB	Carrier 19XR
Design cooling capacity	151 tons	211 tons
Evaporator temperature rise	9.3°C	9.8°C
Condenser temperature rise	9.4°C	10.8°C
Design COP	4.6	4.7
Compressor type	Screw	Centrifugal
Capacity control	Slide Valve	VSD
Evaporator water flowrate	13.50 kg/s	17.79 kg/s
Condenser water flowrate	15.77 kg/s	19.56 kg/s
Refrigerant type	R-22	R-134a

Table 3
Gordon-Ng model fitted parameters for the selected chillers

Item	Water-Cooled Chillers	
	Trane RTHB	Carrier 19XR
ΔS_t^{int}	0.045 kW/K	0.042 kW/K
ΔS_t^{intQ}	0.05 kW/K	-0.05 kW/K
R	0.030 K/kW	0.037 K/kW
$\dot{Q}_t^{leak,eqv}$	89.1 kW	142.8 kW

Table 4
Pumps and fans constants

Item	Chiller	
	Trane RTHB	Carrier 19XR
Primary	5 kW	7 kW
Condenser	4 kW	5 kW
Variable Speed	10 kW	
Tower fan	10 kW	
Coil fan	100 kW	

Table 5
Cooling tower characteristics

Item	Symbol	Value	Note
NTU correlation parameters	c	3.76	Cooling towers based on Dallas/Fort
	n	-0.63	Worth Airport [40]
Design heat rejection capacity	-	360 ton	Each
Design air flowrate	$\dot{m}_t^{twra}$	20 kg/s	At 100% fan speed
Design water flowrate	$\dot{m}_t^{bcw}$	28 kg/s	All chillers are operating
Design tower approach temperature	-	3 °C	Difference between leaving water temperature and wet-bulb temperature
Design wet-bulb temperature	T^{wb}	25 °C	Reference temperature

Table 6
Cooling and dehumidification coil characteristics

Item	Symbol	Value	Note
Coil thermal resistance coefficient	a^1	0.596×10^{-3} K/kg · $m^{\frac{5}{2}}$ · $s^{\frac{15}{4}}$	High-performance coils
	a^2	0.217×10^{-3} K/kg · $m^{\frac{5}{2}}$ · $s^{\frac{15}{4}}$	
	a^3	0.286 K/kW	
Design air flowrate	$\dot{m}^{cca,des}$	120 kg/s	100% fan speed
Max air inlet enthalpy	$h^{ai,des}$	55.6 kJ/kg	27 °C at 50% RH
Design air outlet enthalpy	$h^{ae,des}$	34.1 kJ/kg	12 °C at 100% RH
Air-side temperature drop	-	15 °C	27 °C → 12 °C
Water-side temperature rise	-	13.5 °C	3.5 °C → 16 °C
Coil face area	A^{face}	39 m^2	Normal to air-flow direction
Number of rows	N^{row}	5.1	Thickness of the coils
Design water face velocity	$V^{w,des}$	1 m/s	Normal to flow direction
Design air face velocity	$V^{a,des}$	2.5 m/s	Normal to flow direction

References

[1] F. Jabari, M. Mohammadpourfard, B. Mohammadi-ivatloo, Energy efficient hourly scheduling of multi-chiller systems using imperialistic competitive algorithm, Comput. Electr. Eng. 82 (2020), https://doi.org/10.1016/j.compeleceng.2020.106550 106550.

[2] K.M. Powell, W.J. Cole, U.F. Ekarika, T.F. Edgar, Optimal chiller loading in a district cooling system with thermal energy storage, Energy 50 (1) (2013) 445–453, https://doi.org/10.1016/j.energy.2012.10.058.

[3] J. Deng, S. He, Q. Wei, M. Liang, Z. Hao, H. Zhang, Research on systematic optimization methods for chilled water systems in a high-rise office building, Energy Build. 209 (2020), https://doi.org/10.1016/j.enbuild.2019.109695 109695.

[4] K.P. Lee, T.A. Cheng, A simulation-optimization approach for energy efficiency of chilled water system, Energy Build. 54 (2012) 290–296, https://doi.org/10.1016/j.enbuild.2012.06.028.

[5] M. Ali, V. Vukovic, M.H. Sahir, G. Fontanella, Energy analysis of chilled water system configurations using simulation-based optimization, Energy Build. 59 (2013) 111–122, https://doi.org/10.1016/j.enbuild.2012.12.011.

[6] R. Iru et al., The Optimal Control Strategy for Chilled Water System in Central Air Conditioning Systems, in: 43rd Annual Conference of the IEEE Industrial Electronics Society, 2017, pp. 8150–8155, https://doi.org/10.1109/IECON.2017.8217430.

[7] A.J. Ardakani, F.F. Ardakani, S.H. Hosseinian, A novel approach for optimal chiller loading using particle swarm optimization, Energy Build. 40 (12) (2008) 2177–2187, https://doi.org/10.1016/j.enbuild.2008.06.010.

[8] S. Huang, W. Zuo, M.D. Sohn, Amelioration of the cooling load based chiller sequencing control, Appl. Energy 168 (2016) 204–215, https://doi.org/10.1016/j.apenergy.2016.01.035.

[9] S.R. Thangavelu, A. Myat, A. Khambadkone, Energy optimization methodology of multi-chiller plant in commercial buildings, Energy 123 (2017) 64–76, https://doi.org/10.1016/j.energy.2017.01.116.

[10] Y.C. Chang, Genetic algorithm based optimal chiller loading for energy conservation, Appl. Therm. Eng. 25 (17–18) (2005) 2800–2815, https://doi.org/10.1016/j.applthermaleng.2005.02.010.

[11] D. Zhang, S. Member, P.B. Luh, L. Fellow, J. Fan, S. Member, Chiller Plant Operation Optimization : Primary – Secondary Systems, IEEE Trans. Autom. Sci. Eng. 15 (1) (2018) 341–355.

[12] D. Zhang, P.B. Luh, J. Fan, S. Gupta, Chiller Plant Operation Optimization with Minimum Up/Down Time Constraints, IEEE Robot. Autom. Lett. 3 (1) (2018) 9–15, https://doi.org/10.1109/LRA.2017.2723467.

[13] N. Trautman, A. Razban, J. Chen, Overall chilled water system energy consumption modeling and optimization, Appl. Energy 299 (2021), https://doi.org/10.1016/j.apenergy.2021.117166 117166.

[14] I. Al-Aali, V. Modi, "Examining Ice Storage and Solar PV As a Potential Push Toward Sustainability for Qatar", in *ASME International Mechanical Engineering Congress and Exposition*, Proceedings (IMECE) vol (2018) 6B–2018, https://doi.org/10.1115/IMECE2018-86709.

[15] W.S. Lee, Y.T. Chen, T.H. Wu, Optimization for ice-storage air-conditioning system using particle swarm algorithm, Appl. Energy 86 (9) (2009) 1589–1595, https://doi.org/10.1016/j.apenergy.2008.12.025.

[16] J.A. Candanedo, V.R. Dehkordi, M. Stylianou, Model-based predictive control of an ice storage device in a building cooling system, Appl. Energy 111 (2013) 1032–1045, https://doi.org/10.1016/j.apenergy.2013.05.081.

[17] H.J. Chen, D.W.P. Wang, S.L. Chen, Optimization of an ice-storage air conditioning system using dynamic programming method, Appl. Therm. Eng. 25 (2–3) (2005) 461–472, https://doi.org/10.1016/j.applthermaleng.2003.12.006.
[18] K. Deng et al., Model Predictive Control of Central Chiller Plant With Thermal Energy Storage Via Dynamic Programming and Mixed-Integer Linear Programming, IEEE Trans. Autom. Sci. Eng. 12 (2) (2015) 565–579, https://doi.org/10.1109/TASE.2014.2352280.
[19] D. Rohde, B.R. Knudsen, T. Andresen, N. Nord, Dynamic optimization of control setpoints for an integrated heating and cooling system with thermal energy storages, Energy 193 (2020), https://doi.org/10.1016/j.energy.2019.116771 116771.
[20] Q. Zhu, Q. Li, B. Zhang, L. Wang, G. Li, R. Wang, Capacity optimization for electrical and thermal energy storage in multi-energy building energy system, Energy Procedia 158 (2019) 6425–6430, https://doi.org/10.1016/j.egypro.2019.01.183.
[21] S. Sanaye, A. Shirazi, Thermo-economic optimization of an ice thermal energy storage system for air-conditioning applications, Energy Build. 60 (2013) 100–109, https://doi.org/10.1016/j.enbuild.2012.12.040.
[22] J. Yu, X. Yang, A. Zhao, M. Zhou, Y. Ren, Research on Optimal Control Algorithm of Ice Thermal-Storage Air-Conditioning System, in: Advancements in Smart City and Intelligent Building, 2019, pp. 207–218.
[23] R. Kamal, F. Moloney, C. Wickramaratne, A. Narasimhan, D.Y. Goswami, Strategic control and cost optimization of thermal energy storage in buildings using EnergyPlus, Appl. Energy 246 (April) (2019) 77–90, https://doi.org/10.1016/j.apenergy.2019.04.017.
[24] M. Marghany, "Principles of genetic algorithm," *Synth. Aperture Radar Imaging Mech. Oil Spills*, pp. 169–185, 2020, 10.1016/b978-0-12-818111-9.00010-0.
[25] D.A. Coley, An Introduction to Genetic Algorithms for Scientists and Engineers, An Introd. to Genet Algorithms Sci. Eng. (1999), https://doi.org/10.1142/3904.
[26] P. Bajpai, M. Kumar, Genetic algorithm–an approach to solve global optimization problems, Indian J. Comput. Sci. Eng. 1 (3) (2010) 199–206.
[27] S.T. Taylor, Chilled Water Plant Design Guide, Energy Des. Resour. (2009) 281.
[28] J. McQuiston, F., Parker, J., & Spitler, *Heating, Ventilating and, Air Conditioning*, Sixth. 2005.
[29] S. Hanson, M. Schwedler, and B. Bakkum, "Chiller System Design and Control," 2011.
[31] K. C. ; Ng and Jeffrey M. Gordon, "Cool Thermodynamics : The Engineering and Physics of Predictive, Diagnostic and Optimization Methods for Cooling Systems," *ProQuest Ebook Central*. 2001.
[32] W. Jiang and T. A. Reddy, "Reevaluation of the Gordon-Ng performance models for water-cooled chillers," *ASHRAE Trans.*, vol. 109 PART 2, pp. 272–287, 2003.
[33] M. Hydeman, N. Webb, P. Sreedharan, and S. Blanc, "Development and testing of a reformulated regression-based electric chiller model," *ASHRAE Trans.*, vol. 108 PART 2, pp. 1118–1127, 2002.
[34] P. Haves, Development and testing of a reformulated regression-based electric chiller model: Discussion, ASHRAE Trans. vol. 108 PART 2 (2002) 1127.
[35] P. Hanlon, *Compressor Handbook*. 2020.
[36] ASHRAE, *Chapter 38: Compressors*. ASHRAE, 2020.
[37] P. N. Bali, M. E. Arsana, and P. N. Bali, "Condenser-Evaporator Approach Temperatures and their Influences on Energy Performance of Water Cooled Chillers," in *Proceeding of the 14th International Conference on QIR (Quality in Research)*, 2015, no. June 2018.
[38] C.Y. Chiang, R. Yang, K.H. Yang, The development and full-scale experimental validation of an optimalwater treatment solution in improving chiller performances, Sustain. 8 (7) (2016) 1–21, https://doi.org/10.3390/su8070615.
[39] M.A. Bernier, B. Bourret, Pumping energy and variable frequency drives, ASHRAE J. 41 (12) (1999) 37–40.
[40] J.E. Braun, S.A. Klein, J.W. Mitchell, Effectiveness Models for Cooling Towers and Cooling Coils, ASHRAE Trans. 95 (2) (1989) 164–174.
[41] L. Wang, P. Haves, F. Buhl, An improved simple chilled water cooling coil model, *SimBuild 2012 IBPSA Conference*, 2012.
[42] M.J. Holmes, *The simulation of heating and cooling coils for performance analysis*, in: *1st International Conference on System Simulation in Buildings*, 1982, pp. 245–282.
[43] , Systems" (1997).
[44] T. B. Jekel, "Modeling of ice-storage systems," 1991.
[45] K.H. Drees, Modeling and Control of Area Constrained Ice Storage Systems, Purdue University, West Lafayette, 1994.
[46] J. E. B. Drees, K H, "Modeling and Experimental Validation of Area Constrained Ice Storage Systems," *Int. Refrig. Air Cond. Conf.*, 1994.
[47] D. S. Christian Weber, Ryan Stroupe, "Performance of a Thermal Energy Storage System, 25 Years On," in *Performance of a Thermal Energy Storage System, 25 Years On*, 2015, p. 27.

Further Reading

[30] Daikin, "AG 31-002 Application Guide Centrifugal Chiller Fundamentals," no. February, pp. 1–33, 2015.